Transient energy growth in Two- and Three-dimensional boundary layers

by

Takeo Kuraishi

Kogakushi in Aeronautical Engineering
University of Tokyo (1991)

Submitted to the Department of Aeronautics and Astronautics
in partial fulfillment of the requirements for the degree of

Master of Science in Aeronautics and Astronautics

at the

MASSACHUSETTS INSTITUTE OF TECHNOLOGY

June 1993

Author .....
Department of Aeronautics and Astronautics
February 24, 1993

Certified by .....
Kenneth S. Breuer
Assistant Professor of Aeronautics and Astronautics
Thesis Supervisor

Accepted by .....
Professor Harold Y. Wachman
Chairman, Department Graduate Committee

Transient energy growth in Two- and Three-dimensional boundary layers

by

Takeo Kuraishi

Submitted to the Department of Aeronautics and Astronautics
on February 24, 1993, in partial fulfillment of the
requirements for the degree of
Master of Science in Aeronautics and Astronautics

Abstract

The evolution of localized three-dimensional disturbance in two- and three-dimensional laminar boundary layers is examined. The linearized boundary layer equation is solved using Fourier transforms in the direction parallel to the wall and the Chebyshev collocation technique in the wall-normal direction. A second-order accurate Crank-Nicholson scheme is used to integrate the solution in time, and an LU decomposition and back substitution method is used for matrix inversion.

Spectral analysis of the disturbance shows that substantial short-term growth can be obtained even when the Tollmien-Schlichting waves are damped. This transient growth can reach as much as two or three orders of magnitude, which can then lead to non-linear interaction and breakdown to turbulent flow. This mechanism can bypass the traditional instability mechanism involving the Tollmien-Schlichting waves.

The initial vertical velocity is set to the least-damped discrete mode and the initial vertical vorticity is set to zero, which will give large transient energy growth. The waves that give the largest transient growth are those with streamwise wave number $\alpha \simeq 0$. The maximum energy obtained is found to depend on the initial linear growth of the vorticity energy component, the decay rate Ci, and the ratio of the vertical velocity and vorticity energy of the least damped eigenfunction. Additional instability in three-dimensional boundary layers can occur due to inflectional instability of the crossflow profile. Thus, modes with low α become less stable and exhibit even larger transient energy growth.

Thesis Supervisor: Kenneth S. Breuer
Title: Assistant Professor of Aeronautics and Astronautics

Contents

List of Figures

Nomenclature

U_0	Velocity of the inviscid flow.
x	Local direction tangent to U_0. 'Streamwise direction'
y	Local direction normal to the wall. 'Vertical direction'
z	Local direction parallel to the wall and normal to x 'Crossflow direction'.
ψ	Local sweep angle of the inviscid flow from the chord direction.
δ^*	Displacement thickness. $\delta^* = \int_0^\infty (1 - U(y))dy$.
$U(y)$	Mean streamwise velocity, non-dimensionalized by U_0 to be equal to 1 outside the boundary layer.
V	Mean vertical velocity, $= 0$.
$W(y)$	Mean crossflow velocity, non-dimensionalized by U_0.
u	Streamwise velocity perturbation.
v	Vertical velocity perturbation.
w	Crossflow velocity perturbation.
p	Perturbation pressure non-dimensionalized by ρU_0^2.
t	Time non-dimensionalized by δ^*/U_0.
Re	Reynolds number based on displacement thickness. $Re_{\delta^*} = (U_0\delta^*)/\nu$

α	Wavenumber for Fourier transform in the x-direction.
β	Wavenumber for Fourier transform in the z-direction.
k	Wavenumber in the wave vector direction.
	$k^2 = \alpha^2 + \beta^2$.
$\tilde{v}(\alpha, \beta)$	Fourier transform of v for a set of α and β.
$\tilde{u}(\alpha, \beta)$	Fourier transform of u.
$\tilde{w}(\alpha, \beta)$	Fourier transform of w.
$\tilde{\eta}(\alpha, \beta)$	Fourier transform of the vertical vorticity for a set of α and β.
	$\tilde{\eta} = \imath(\beta\tilde{u} - \alpha\tilde{w})$
E	Total kinetic energy of the perturbation for a set of α and β.
	$E = \int_0^\infty \lvert\tilde{v}\rvert^2 + \frac{1}{k^2}(\lvert\tilde{\eta}\rvert^2 + \lvert\tilde{v'}\rvert^2)dy$
H	Hartree parameter used for the Falkner-Skan-Cooke transformation.
	$H = 2m/(m+1)$
l	Mapping factor for the Chebyshev collocation method.

Acknowledgement

I would like to thank my advisor Professor Kenny Breuer for his advice and help. He has provided me with guidance through this whole process, without which I would still be lost and confused.

I would also like to thank my former advisor Professor Morishita and Professor Aihara at University of Tokyo for their encouragement and support.

Special thanks to my colleagues in the Computational Aerospace Sciences Laboratory. They have been most helpful and encouraging. I am proud to have been a member of that lab. It has been an immensely enjoyable time.

My deepest gratitude goes to my parents who have paid for my study here at MIT. They have provided me with the opportunity to fulfill my dream, and I will not let them down.

Thank you all.

Chapter 1

Introduction

1.1 Background

1.1.1 Transition in two-dimensional boundary layers

An important phenomenon in fluid dynamics is the transition of a laminar boundary layer to a turbulent flow. Traditional approaches to the prediction of the transition have been based on the study of the evolution of Tollmien-Schlichting (T-S) waves, which are governed by the Orr-Sommerfeld equation. This equation can be solved as an eigenvalue problem, with the eigenvalues determining whether the waves grow or decay. For a two-dimensional boundary layer such as a Blasius flow, Squire's theorem shows that any three-dimensional problem can be reduced to an equivalent two-dimensional problem at a lower Reynolds number. Therefore, one can expect the two-dimensional waves to become unstable before three-dimensional waves do, and for this reason, most studies on instability have concentrated on the behavior of two-dimensional waves. The instability of these waves is often known as streamwise or viscous instability.

The T-S waves initially evolve linearly, and this is known as the primary instability. As these waves amplify, they exhibit spanwise variations from interactions between the waves and the mean flow . This is known as the secondary instability and take the form of three-dimensional waves and streamwise vortices. These three-dimensional

formations breakdown in cascades, eventually becoming fully turbulent flows. (See Klebanoff, Tidstrom, and Sargent [13], Craik [5], and Herbert [11].)

1.1.2 Transition in three-dimensional boundary layers

A three-dimensional boundary layer flow such as the flow over a swept wing exhibits transition behaviors different from those of the two-dimensional boundary layers, which are characterized by a crossflow component in addition to the main flow. The crossflow instability was first observed by Gray [6] in 1952, who observed closely spaced stationary streaks in the local flow direction behind the laminar region near the leading edge. Experiments conducted using wings, cylinders, and flat plates show that the streamwise vortices are amplified most in the region of high pressure gradient; traveling waves of around 1 kHz being amplified more than stationary waves. In addition, non-linear interactions between the waves and the distorted mean flow can occur. However, these are not yet fully understood. (See Saric and Reed [18] for a complete review of theories and experiments.)

The crossflow instability is due to the inflectional velocity profile of the crossflow. Rayleigh's inflectional criterion shows that for inviscid flows, any flow with an inflection point is unstable. An inflectional velocity profile causes instability even in viscous flows if the Reynolds number is large enough. The direction of the least stable wave is generally in the crossflow direction.

A comprehensive article by Mack [15] presents problem formulation, results, and physical mechanisms on stability in both two- and three-dimensional boundary layers. He has shown the relationship between the critical Reynolds number, the pressure gradients, and the sweep angles for both the incompressible and compressible three-dimensional boundary layers. When the crossflow component is small enough, the critical Reynolds number where the flow becomes unstable is determined by the streamwise (T-S) instability. The direction of the least stable wave is within a few degrees of the streamwise direction. However, when the crossflow component is larger, the critical Reynolds number is determined by the stability of the waves in the crossflow direction, which is where the least stable wave is found.

1.1.3 Transient growth and bypass transition

Even though traditional stability theory has corresponded well with experiments in which waves are forced by a vibrating ribbon or heating element, it is not sufficient to explain all phenomenon in the actual transition. The initial disturbances might be three-dimensional in nature and can immediately lead to turbulent flow, often bypassing the primary instability. These kinds of transitions are known as "bypass transitions".

Traditional linear stability theory examines only the vertical velocity perturbation, and the horizontal velocity perturbation is assumed to be secondary in nature. However, Landahl [14] has shown that for an initial disturbance of three-dimensional nature, any inviscid shear flow can exhibit at least a linear growth in kinetic energy. An initial disturbance which has a vertical velocity component with spanwise variation will result in a displacement of fluids of different velocities. This "liftup" will result in the formation of a shear layer, which may grow even if the vertical disturbance decays. Hultgren and Gustavsson [12] showed that for the viscous case, the short-time growth of the horizontal velocity resulting from a disturbance infinitely elongated in the streamwise direction is nearly linear, while the long-term behavior shows decay resulting from viscosity.

Based on the work by Landahl, Breuer and Haritonidis [2] examined experimentally and analytically the evolution of a three-dimensional impulsive disturbance in a laminar boundary layer and the subsequent breakdown to turbulence. Their results initially showed nearly linear growth of the horizontal perturbation for both the inviscid calculation and the experiment. A shear layer developed, which was advected downstream at the local velocity. It was tilted and stretched in the streamwise direction, intensifying as the disturbance evolved, until finally being dissipated by viscosity. However, the amplitude that the horizontal velocity attained in a short time far exceeded the initial vertical velocity amplitude. This short-term growth was referred to as the "transient part" by Breuer and Haritonidis. This thesis will refer to it in the same way.

Henningson [10] and Gustavsson [9] have examined the energy growth for the

viscous plane Poiseuille flow. Henningson has examined the growth of the vertical vorticity and its mechanism using eigenfunction expansion. He showed that the transient growth was due to the inhomogeneous nature of the Squire equation. Furthermore, the maximum growth of the vertical vorticity is $\mathcal{O}(Re)$ and is obtained in time $\mathcal{O}(Re)$. Gustavsson examined the maximum energy amplification obtained when the Orr-Sommerfeld modes were used as the initial vertical velocity and the vertical vorticity was set to zero. He showed that the maximum is obtained when the initial vertical velocity corresponding to the least damped Orr-Sommerfeld mode, with its structure infinitely elongated in the streamwise direction, is used.

Butler and Farrell [3] examined same kinds of flows to obtain the optimal disturbance which gives the maximum energy growth. They showed that this optimal disturbance is also obtained for disturbance infinitely elongated in the streamwise direction and that is a combination of linearly dependent eigenmodes.

The transient growth can be described as the liftup of vortex tubes and its subsequent tilting and stretching. The mean flow has vortex tubes which are normal to the mean flow direction. A vertical movement of the fluid will lift up a section of this tube, changing its orientation. Thus, some of the vorticity component in the crossflow direction will be translated to the vertical vorticity component, causing the initial growth of vertical vorticity. The vortex tube will then be tilted and stretched as it is advected downstream at the local mean velocity. If the vertical velocity decays, the liftup effect will lessen in time. Therefore, the vortex tube will not receive more energy, and will subsequently be dissipated by viscous effect. This transient growth appear as streak-like regions of high and low speed streamwise velocity if it is viewed in the xz-plane and as as inclined shear layer in the xy-plane.

This transient growth is strongly dependent on the initial condition, and is best when the initial condition has strong spanwise features with small variation in the streamwise direction. Results of research by Henningson, Gustavsson, and Butler and Farrell show that the maximum vertical vorticity amplitude is obtained for modes with $\alpha = 0$ (streamwise vortices), with the initial vertical vorticity set to zero. Even when the linear stability theory predicts decay, this growth can be of two or three orders

of magnitude, which can then lead to non-linear interactions and the breakdown of the laminar flow before the traditional theory of the streamwise T-S waves predicts transition.

The disturbances that result in large transient growth are streamwise vortices which distort the mean flow, causing spanwise variation in the streamwise velocity. Traditionally, formation of three-dimensional structures were assumed to be secondary in nature, occurring due to non-linear interactions between the T-S waves after they attain a certain amplitude. However, as noted by Breuer and Haritonidis [2] and by Butler and Farrell [3], this transient growth has the same mechanism as the secondary instability, but evolves rapidly and is a linear process. The similarity indicates that this approach to transition study may be quite valid. It is quite possible that such secondary instability can be analyzed using linear methods.

1.2 Present approach

In this project, the work by Breuer and Haritonidis [2] is extended to viscous disturbances in both two- and three-dimensional boundary layers. This is motivated by the fact that modern aircrafts employ a swept wing, which has different stability and transition characteristics because of the existence of crossflow. The inflection of the crossflow velocity profile will lead to crossflow instability, which is expected to affect the behavior of the three-dimensional disturbances.

In addition to examining the physical evolution of the localized disturbance, the evolution of each Fourier mode will be examined. The Fourier mode that gives the largest energy growth will be obtained, as will the initial condition that gives the maximum transient growth and the amount of amplification. The effects of the Reynolds number, the sweep angle, and the pressure gradient on the transient growth will also be examined.

Chapter 2

Theory

2.1 Boundary layers on swept wings

A well-known example of the three-dimensional flow in aeronautical applications is the boundary layer over a swept wing, in which the pressure gradient exists not only in the direction tangent to the flow but also in the direction normal to the flow, bending the flow toward the lower pressure region (figure 2-1). An important feature of this kind of flow is the existence of a crossflow velocity, present due to the fact that the low speed flow near the wall is affected more strongly by the pressure gradient and is therefore more bent than the inviscid flow outside the boundary layer (figure 2-2).

The coordinate system is defined locally as shown in figure 2-1. The x-direction is parallel to the wall and in the same direction as the local inviscid flow outside the boundary layer. The y-direction is normal to the wall; the z-direction is normal to both the x- and y-direction. The local sweep angle ψ is the angle between the x-direction and the chord direction. The x-,y-, and z-direction will be referred to as the 'streamwise', 'vertical', and 'crossflow' direction respectively. The velocities are defined as follows: U and W represent the mean velocities in the x- and z-directions, while the mean vertical velocity V is zero. u, v, and w represent the three perturbation velocities in the x-,y-, and z-directions respectively. The displacement thickness, δ^*, calculated from the streamwise velocity profile and the inviscid velocity, U_0, are used for non-dimensionalization.

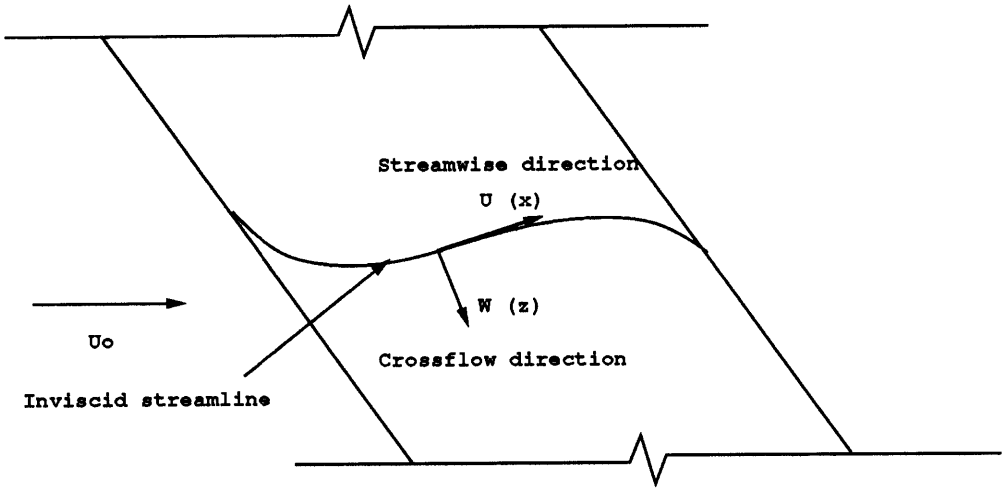

Figure 2-1: Schematic of the inviscid streamline over an infinite swept wing.

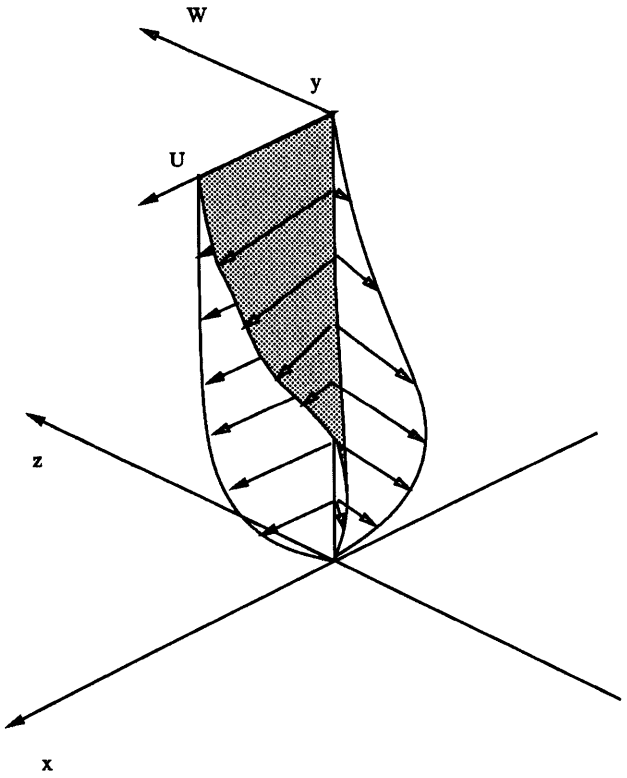

Figure 2-2: Schematic of the velocity components of a boundary layer over a swept wing.

2.2 Equations for three-dimensional boundary layers

Some assumptions will be necessary to derive the equations of motion. First, the boundary layer growth can be assumed to be small enough to be disregarded. We can then assume that the mean velocity remains constant in the x- and z-directions and that the mean vertical velocity is zero. Secondly, we assume that perturbation velocities are small enough relative to the mean flow that quadratic terms of the perturbation can be dropped.

The Navier-Stokes equations are linearized and transformed to Fourier space in the x- and z-directions using the wavenumbers α and β . This leads to the Orr-Sommerfeld equation and the Squire equations:

$$[\frac{\partial}{\partial t} + i(\alpha U + \beta W)](\frac{\partial^2}{\partial y^2} - k^2)\tilde{v} - i(\alpha U'' + \beta W'')\tilde{v} - \frac{1}{Re}(\frac{\partial^2}{\partial y^2} - k^2)^2\tilde{v} = 0, \quad (2.1)$$

$$[\frac{\partial}{\partial t} + i(\alpha U + \beta W) - \frac{1}{Re}(\frac{\partial^2}{\partial y^2} - k^2)]\tilde{\eta} = i(\alpha W' - \beta U')\tilde{v}, \quad (2.2)$$

$$k^2 = \alpha^2 + \beta^2, \quad (2.3)$$

where $\tilde{v}$ and $\tilde{\eta}$ represent the transformed qualities of the vertical velocity v and the vertical vorticity η, while k represents the combined wavenumber. The Orr-Sommerfeld and Squire equations require four and two boundary conditions respectively. The wall is a solid boundary with no forcing of the vertical component. while continuity requirement sets v' to zero at the wall, since both u and w are zero at all locations on the wall. All perturbations are bounded and decay exponentially in the free stream so that v and v' go to zero at infinity. The vorticity is also zero at the wall and decays exponentially in the freestream to zero at infinity. More details of the derivation are given in Appendix A.1.

If we replace the time derivatives with temporal eigenvalues, then both equations can be solved as eigenvalue problems. The real part of the eigenvalue will give the phase of the eigenmode, while the imaginary part will show the decay or growth rate.

The Orr-Sommerfeld equation is a homogeneous equation. Given initial and boundary conditions, it can be solved without any knowledge of the horizontal velocity. On the other hand, the Squire equation is inhomogeneous with a forcing term due to the vertical velocity. The solution to this equation will have two components. One is the homogeneous part which is independent of the forcing term, and the other is the particular part which depends on the vertical velocity. It can be shown that the homogeneous solution of the Squire equation always decays. However, the particular part will have the same decay rate as the corresponding vertical velocity and may grow or decay.

It can be seen that the $\alpha U + \beta W$ term and its second derivative in (2.1) can be replaced by a corresponding αU_{2D} to reduce the equation for a three-dimensional boundary layer to a two-dimensional one. When W or α is small enough to be disregarded, (2.2) can also be reduced to a two-dimensional equation, so that we can expect the solutions of the equations to be nearly identical. However, when we examine the case where W is larger and α is smaller, we can see that the corresponding two-dimensional mean flow profile will have an inflectional point, which will make waves with low α and high β less stable.

We can make some predictions as to how the velocity and the vorticity will evolve given an initial vertical velocity that corresponds to a slowly decaying eigenfunction. The vertical velocity will decay exponentially as predicted by the Orr-Sommerfeld equation. The vertical vorticity on the other hand, may exhibit transient growth as the vertical vorticity is forced by the right-hand side of the Squire equation. However, as the vertical vorticity becomes larger, the homogeneous solution which is responsible for the transient behavior will decay, leaving only the particular solution, which have the same decay rate as the vertical velocity. Our interest however, is not in how the vertical vorticity behaves after a long time, but rather how it will evolve initially and how much energy it can gain.

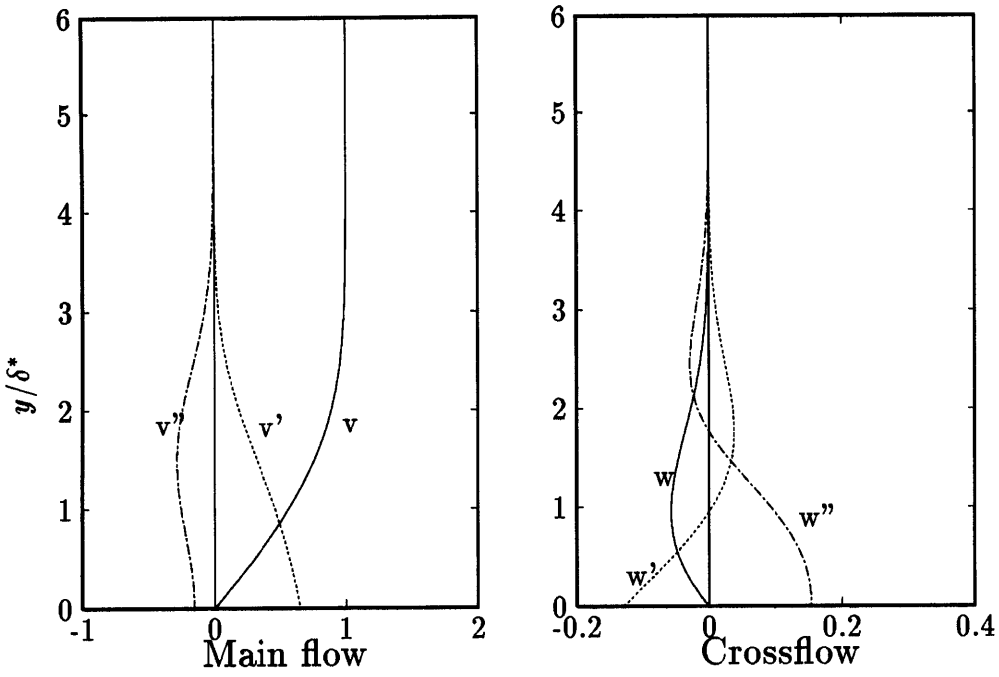

Figure 2-3: The mean flow profile generated by the Falkner-Skan-Cooke transformation. $\psi = 45^0, H = 0.3$. Note the inflectional velocity profile for the crossflow.

2.3 Falkner-Skan-Cooke boundary layers

In order to examine the stability of a flow over a swept wing, it is necessary to have a set of mean flow profiles for a given sweep angle and pressure gradient. We have followed the method given in Rosenhead [19] and Mack [15], which uses the Falkner-Skan-Cooke transformation [4].

Cooke extended the familiar Falkner-Skan transformation for calculating the two-dimensional velocity profile of flow over a wedge to an infinite wedge with sweep. The two parameters used by Cooke are the Hartree parameter, H, which is $1/\pi$ of the wedge angle (as in the usual Falkner-Skan transformation), and the sweep angle, ψ, which is the sweep angle of the wedge to the free stream.

The flow over the wedge is divided into two components: one normal to and the other tangent to the leading edge. The boundary layer equation for the normal direction reduces to the familiar Falkner-Skan equation, while the equation for the flow tangent to the leading edge is dependent on the velocity profile in both directions. The resulting velocity profiles are combined to give the streamwise and crossflow velocity

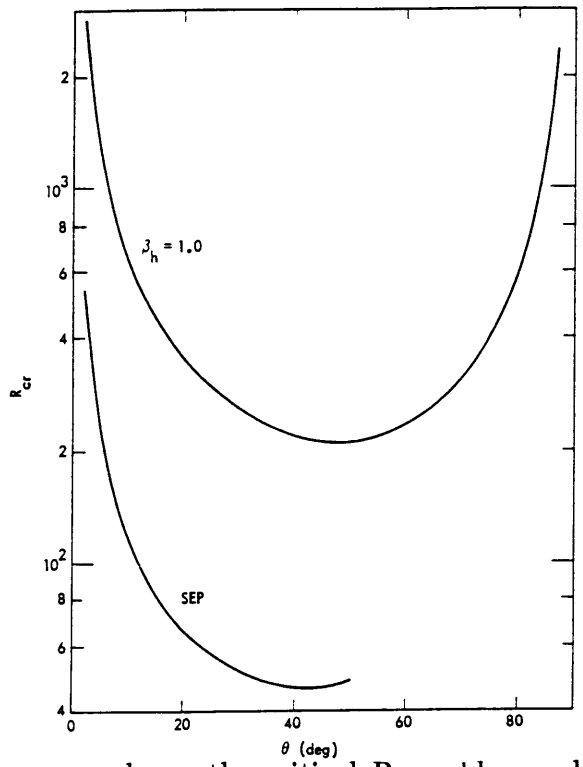

Figure 2-4: Effect of sweep angle on the critical Reynolds number for crossflow instability of Falkner-Skan-Cooke boundary layers at $H = 1.0$ and $H = -0.199$. From Mack [15]

profiles. The equations for transformation and some calculated velocity profiles are given in the Appendix A.2.

Figure 2-3 shows the streamwise and the crossflow velocity profile for $\psi = 45^0$ and $H = 0.3$. The effect of the sweep angle is to make the streamwise flow 'thinner' if $H > 0$ or 'fatter' if $H < 0$. The crossflow velocity profiles, which have the same shape regardless of ψ, always has an inflection point. The crossflow is largest when $H = 1$, which is the velocity profile along the stagnation line, or when $H = -0.198837$, which corresponds to a separating flow. The effect of the sweep angle is to make this crossflow profile larger or smaller, with the maximum crossflow velocity at $\psi = 45^0$.

Experiments have shown that the crossflow instability usually becomes apparent in the accelerated flow region of the wing. Therefore, for most of the analysis, flows with the Hartree parameter H between 0.0 and 0.5 have been examined. In addition, the sweep angle of 45^0 is used since it gives the largest crossflow velocity and is likely to exhibit the effect of both the streamwise and crossflow instability.

Figure 2-4 and figure 2-5 show the critical Reynolds number according to the linear

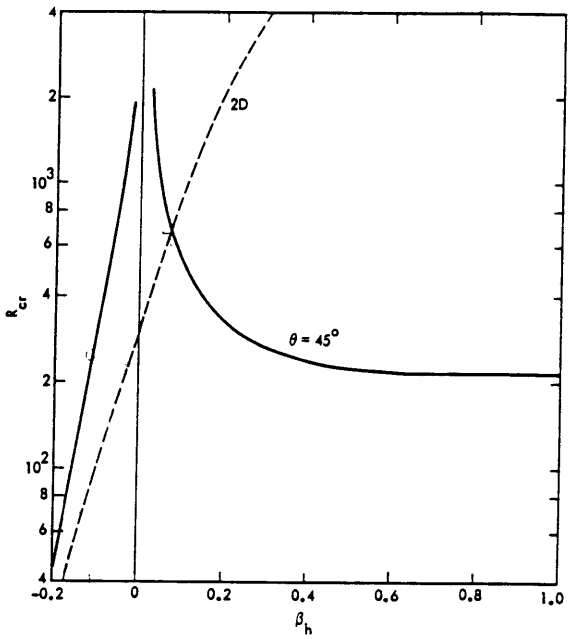

Figure 2-5: Effect of pressure gradient on critical Reynolds number. The solid line indicates crossflow instability for Falkner-Skan-Cooke boundary layer with $\psi = 45^0$; the dashed line indicates the two-dimensional Falkner-Skan boundary layer. From Mack [15]

instability theory calculated by Mack [15] using these velocity profiles. Figure 2-4 shows the relationship of the critical Reynolds number and the sweep angle for Falkner-Skan-Cooke boundary layers. We can see that the lowest Reynolds number is obtained when the sweep angle ψ is near 45^0, due to the fact that the crossflow component has the largest amplitude when $\psi = 45^0$. The critical Reynolds number for crossflow instability with a sweep angle of $\psi = 0^0$ and $\psi = 90^0$ is at infinity since they have no crossflow component.

Figure 2-5 shows the critical Reynolds numbers for both the two-dimensional instability and the crossflow instability for various values of the Hartree parameter. While the critical Reynolds number increases with the Hartree parameter for the two-dimensional Falkner-Skan boundary layer, the critical Reynolds number for the Falkner-Skan-Cooke boundary layer at a sweep angle 45^0 decreases as the Hartree parameter increases. This is especially important for a higher H, where the critical Reynolds number for the swept wing is far smaller than that of the two-dimensional

boundary layer.

For three-dimensional boundary layers with a sweep angle of 45^0, the critical Reynolds number for crossflow instability becomes lower than the critical Reynolds number for streamwise instability at around $H = 0.07$. Therefore, we can expect the crossflow instability to occur first for the Falkner-Skan-Cooke boundary layers with $H > 0.07$.

Chapter 3

Numerical Scheme

3.1 Time integration

The implicit and second order accurate Crank-Nicholson scheme was used for the time integration. The finite difference equations for the Orr-Sommerfeld (2.1) and Squire (2.2) equations are

$$\nabla^2\tilde{v}^{n+1} - \nabla^2\tilde{v}^n = [\frac{i\triangle t}{2}(\alpha U'' + \beta W'') - \frac{i\triangle t}{2}(\alpha U + \beta W)\nabla^2 + \frac{\triangle t}{2Re}\nabla^4](\tilde{v}^{n+1} + \tilde{v}^n), \quad (3.1)$$

$$\tilde{\eta}^{n+1} - \tilde{\eta}^n = [\frac{i\triangle t}{2}(\alpha U + \beta W) - \frac{\triangle t}{2Re}\nabla^2](\tilde{\eta}^{n+1} + \tilde{\eta}^n) - \frac{i\triangle t}{2}(\alpha W' - \beta U')(\tilde{v}^{n+1} + \tilde{v}^n), \quad (3.2)$$

where

$$\nabla^2\tilde{v} = (\frac{\partial^2}{\partial y^2} - k^2)\tilde{v}, \quad (3.3)$$

$$\nabla^4\tilde{v}^n = (\frac{\partial^4}{\partial y^4} - 2k^2\frac{\partial^2}{\partial y^2} + k^4)\tilde{v}^n. \quad (3.4)$$

These equations were marched forward in time using the time step of $\triangle t = 0.1$, yielding results that were acceptably accurate, matching analytic results to four or five significant digits.

3.2 Chebyshev collocation method

In order to calculate the fourth-order derivatives in y accurately, Chebyshev polynomials were used to approximate the functions $\tilde{v}$ and $\tilde{\eta}$. Chebyshev polynomials are defined in ξ between -1 and 1 as follows:

$$T_0(\xi) = 1, \tag{3.5}$$

$$T_1(\xi) = \xi, \tag{3.6}$$

$$T_2(\xi) = 2\xi^2 - 1, \tag{3.7}$$

...

$$T_{k+1}(\xi) = 2\xi T_k(\xi) - T_{k-1}(\xi) \qquad (k \geq 1). \tag{3.8}$$

These polynomials can also be written as

$$T_k(\xi_j) = \cos\{k \arccos(\xi_j)\} \qquad (j = 0, ..., N). \tag{3.9}$$

If we choose ξ such that $\xi_j = \cos(j\pi/N)$ where N is the number of the polynomials, the polynomials become

$$T_k(\xi_j) = \cos(\frac{jk\pi}{N}) \qquad (j = 0, ..., N). \tag{3.10}$$

Therefore, the discrete values of $\tilde{v}$ and $\tilde{\eta}$ at $\xi_j = \cos(j\pi/N)$ will be used for the collocation. The value of $\tilde{v}$ at ξ_j can be represented in the following manner:

$$\tilde{v}_j = \mathbf{T}_j^T \tilde{\mathbf{v}}^n, \tag{3.11}$$

where $\mathbf{T}_j^T$ is the transposed Chebyshev polynomial array for ξ_j and $\tilde{\mathbf{v}}^n$ is the coefficient array.

We can easily obtain the ξ-derivatives of the function by using the derivatives of the polynomials. These derivatives of the polynomials are obtained by the equation,

$$2T_k^{(n)} = \frac{1}{k+1}T_{k+1}^{(n+1)} - \frac{1}{k-1}T_{k-1}^{(n+1)} \qquad (k \geq 1). \tag{3.12}$$

3.3 Domain mapping

Since the actual domain of y is between 0 and ∞, it is necessary to map this to ξ. This was done using an algebraic mapping function:

$$\xi = \frac{l-y}{l+y}. \tag{3.13}$$

The mapping factor, l, should be set so that the mapping concentrates the points in the region with an interesting phenomenon. This scheme is very accurate for describing a localized phenomenon in the boundary layer region but is inadequate for describing a phenomenon that takes place outside the boundary layer or that has a structure that extends from near the wall to outside the boundary layer. The solution calculated for the discrete modes using l from 1 to 10 remained accurate and matched quite well. However, in order to represent the phenomenon accurately and in detail, l has been set to 1 or 2 in most cases.

The y derivatives are also modified according to the mapping:

$$\frac{\partial f}{\partial y} = -\frac{2\psi^2}{l}\frac{\partial f}{\partial \xi}, \tag{3.14}$$

$$\psi = \frac{\xi+1}{2}, \tag{3.15}$$

$$\frac{\partial^2 f}{\partial y^2} = \frac{4\psi^4}{l^2}\frac{\partial^2 f}{\partial \xi^2} + \frac{4\psi^3}{l^2}\frac{\partial f}{\partial \xi}, \tag{3.16}$$

$$\frac{\partial^4 f}{\partial y^4} = \frac{16\psi^5}{l^4}(\psi^3\frac{\partial^4 f}{\partial \xi^4} + 6\psi^2\frac{\partial f^3}{\partial \xi^3} + 9\psi\frac{\partial f^2}{\partial \xi^2} + 3\frac{\partial f}{\partial \xi}). \tag{3.17}$$

For example, the second derivative of $\tilde{v}$ at y_j can be obtained by using the coeffi-

cient array $\tilde{\mathbf{v}}^n$:

$$\frac{\partial^2 \tilde{v}^n}{\partial y^2} |_{y_j} = (\frac{4\psi^4}{l^2}\mathbf{T}''^T_j + \frac{4\psi^3}{l^2}\mathbf{T}'^T)\tilde{\mathbf{v}}^n, \tag{3.18}$$

where $\mathbf{T}'^T_j$ and $\mathbf{T}''^T_j$ represent the first and the second derivatives of Chebyshev polynomials at ξ_j.

3.4 Matrix formulation

Using the Chebyshev polynomials, (3.1) and (3.2) can be written in matrix form for the arrays $\tilde{\mathbf{v}}^n$ and $\tilde{\boldsymbol{\eta}}^n$ which represent the coefficients for the complete vertical velocity and vorticity perturbations at the time step n. After some matrix operation, we obtain for $\tilde{\mathbf{v}}^n$:

$$(\mathbf{D}+i\mathbf{RD}-i\mathbf{S}-\mathbf{PD}^2)\tilde{\mathbf{v}}^{n+1} = (\mathbf{D}-i\mathbf{RD}+i\mathbf{S}+\mathbf{PD}^2)\tilde{\mathbf{v}}^n, \tag{3.19}$$

where $\mathbf{R}$, $\mathbf{S}$ and $\mathbf{P}$ represent the diagonal matrices associated with the mean profile.

$$\mathbf{R} = \frac{\triangle t}{2}(\alpha U_j + \beta W_j)\mathbf{I}, \tag{3.20}$$

$$\mathbf{S} = \frac{\triangle t}{2}(\alpha U''_j + \beta W''_j)\mathbf{I}, \tag{3.21}$$

$$\mathbf{P} = \frac{\triangle t}{2Re}\mathbf{I}. \tag{3.22}$$

$\mathbf{D}$ is the polynomial matrix associated with the Laplacian derivative in the normal direction (3.3), $\mathbf{D}^2$ is the polynomial matrix associated with the double Laplacian derivative in the normal direction (3.4), and $\mathbf{I}$ is the identity matrix.

The equation (3.2) for the array $\tilde{\boldsymbol{\eta}}^n$, which is the coefficients for the normal vorticity $\tilde{\eta}$, can also be written in the matrix form:

$$(\mathbf{I}+i\mathbf{R}-\mathbf{PD})\tilde{\boldsymbol{\eta}}^{n+1} = (\mathbf{I}-i\mathbf{R}+\mathbf{PD})\tilde{\boldsymbol{\eta}}^n - i\mathbf{Q}(\tilde{\mathbf{v}}^{n+1}+\tilde{\mathbf{v}}^n), \tag{3.23}$$

where matrices $\mathbf{R}$ and $\mathbf{P}$ are as defined above and $\mathbf{Q}$ is another constant diagonal

matrix:

$$\mathbf{Q} = \frac{\triangle t}{2}(\beta U' - \alpha W')\mathbf{I}. \tag{3.24}$$

This equation was also integrated at the same time as the Orr-Sommerfeld equation using the current values for $\tilde{\mathbf{v}}^n$ and $\tilde{\mathbf{v}}^{n+1}$.

We calculated the subsequent vertical disturbance velocity by applying the matrices to the $\tilde{\mathbf{v}}^n$ array iteratively. LU decomposition and back substitution method was used for matrix calculation. For fixed α, β and $\triangle t$, all of the matrices are constant and need to be calculated only once at $t = 0$, which makes the LU method practical. The matrices, after being decomposed once, were then repeatedly used in the back substitution, saving redundant calculation. The calculation count is at least $\frac{1}{3}N^3$ for the initial decomposition and $\frac{1}{6}N^2$ for subsequent back substitutions.

Values between 32 and 128 were used in the calculation. While increasing N theoretically raises the accuracy, roundoff error of the computer imposes a practical limit as shown by Breuer and Everson [1]. In general, 64 was used to balance between speed and accuracy. In addition, the magnitude of some coefficients grew quite large. This was especially true for some special cases, such as when $\alpha = 0$.

3.5 Details

The computation was carried out on a DEC station 3100. For integrating a localized disturbance with 32 points in the x- and z-direction, 64 Chebyshev polynomials, 1000 time steps, and at single precision, the CPU time required was approximately 6 hours.

Calculation using both single precision and double precision showed that double precision was unnecessary in most cases. Therefore, most cases were calculated using single precision. The cases that required double precision were those with longer periods of integration, those with small α, or those having 128 Chebyshev polynomials.

The vertical velocity and the vertical vorticity were transformed to Fourier space, where each Fourier mode was calculated independently. The results were then transformed to physical space using Fast Fourier Transforms.

In addition, the behavior of each Fourier mode were examined in detail. This was

done by examining the total perturbation energy and its components. The energy is defined as follows:

$$E = \int_0^\infty (\tilde{v}^2 + \tilde{u}^2 + \tilde{w}^2) dy. \tag{3.25}$$

This is equivalent to the following equation due to the relation given in the Appendix A.1.

$$E = \int_0^\infty |\tilde{v}|^2 + \frac{1}{k^2}(|\tilde{\eta}|^2 + |\tilde{v'}|^2) dy. \tag{3.26}$$

Chapter 4

Modal Studies

4.1 Initial conditions

Any given initial condition can be represented as a combination of eigenfunctions. Since the least damped mode will dominate the long-time solution, it is natural to examine the temporal evolution of the energy using this eigenfunction as the initial condition. These eigenfunctions are three-dimensional in nature, having horizontal as well as vertical velocity components. In the following computations, both the vertical velocity and the vertical vorticity need to be specified for initial conditions. The temporal behavior of the vertical velocity can be easily estimated by its eigenvalues. However, as we have seen in Section 2.2, the behavior of the vertical vorticity part depends on both the vertical velocity and the initial vorticity. Previous works on Poiseuille flow have shown that the maximum energy growth is obtained when the initial vertical vorticity is set to zero, and we can expect similar results for boundary layer flow.

For two- and three-dimensional boundary layer velocity profiles, the least damped mode typically has a simple profile, as shown in figure 4-1. The solid and the dotted lines represent the amplitude of the vertical velocity and the vertical vorticity for the least damped mode, respectively. We can see that η has a larger maximum compared to v. For waves with k less than 1, the ratio of vorticity energy and the velocity energy will be even larger.

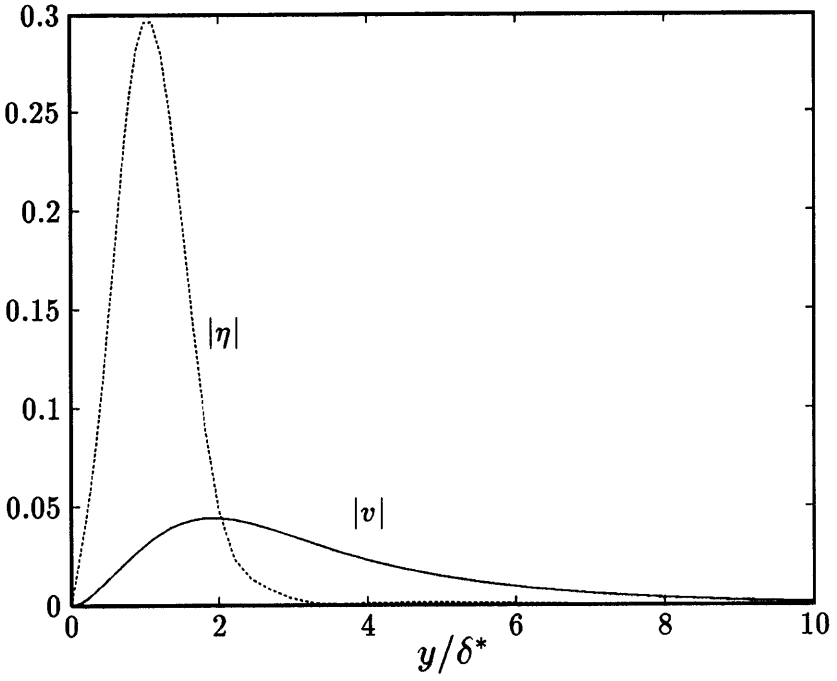

Figure 4-1: Eigenfunction of a least damped mode. $\psi = 45^0, H = 0.3, Re = 500, \alpha = 0.2, \beta = 0.4$. The η component has larger amplitude than v but is confined within the boundary layer.

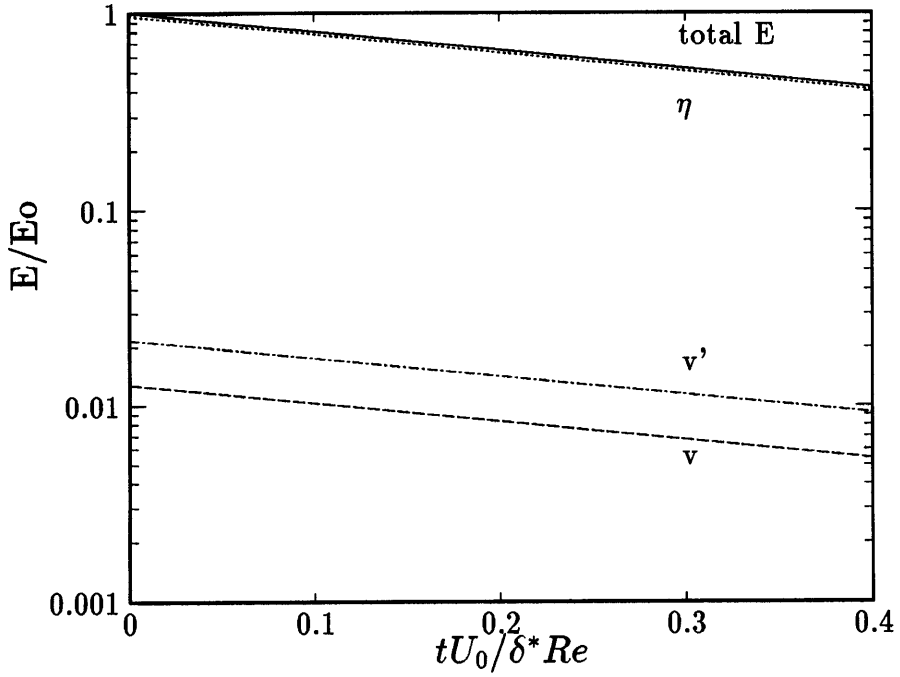

Figure 4-2: Temporal behavior of the total energy and its components with non-zero initial vertical vorticity. $\psi = 45^0, H = 0.3, Re = 500, \alpha = 0.2, \beta = 0.4$. The vertical velocity and vorticity decay exponentially at the same rate.

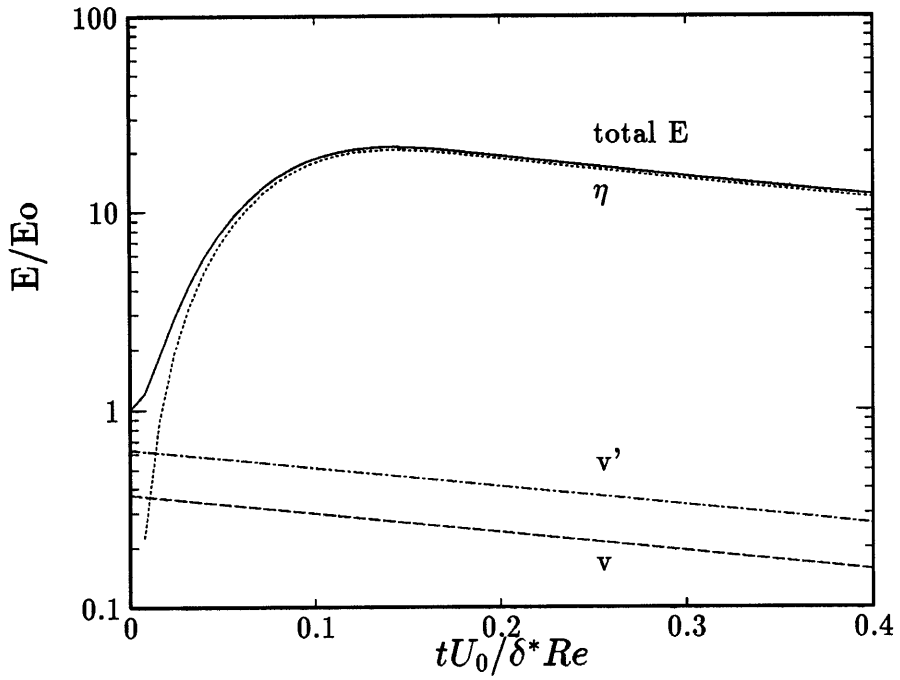

Figure 4-3: Temporal evolution of the total energy and its components with zero initial vertical vorticity. $\psi = 45^0, H = 0.3, Re = 500, \alpha = 0.2, \beta = 0.4$. The energy grows to 25 times the original energy, with most contribution from the vertical vorticity part.

Figure 4-2 shows the time evolution of the energy and its components when the complete mode of the least damped eigenfunction is used as the initial disturbance. Since this eigenfunction corresponds to the particular solution of the Squire equation, the energy and its components will decay exponentially at the same rate, so that the ratio of the energy amplitude of the vertical vorticity and the vertical velocity will remain constant. This ratio can be calculated from the initial eigenfunction shown in figure 4-1.

4.2 Evolution of $\eta_0 = 0$ mode

Instead of a complete mode, we can set $\eta_0 = 0$, in which case we can expect transient growth due to the forcing of the Squire equation. Figures 4-3 and 4-4 show the temporal evolution of modes that decay and grow. Figure 4-3 shows the evolution of the energy and its component when the same initial vertical velocity as in figure 4-2 is used, but with the initial vertical vorticity set to zero. The vertical velocity

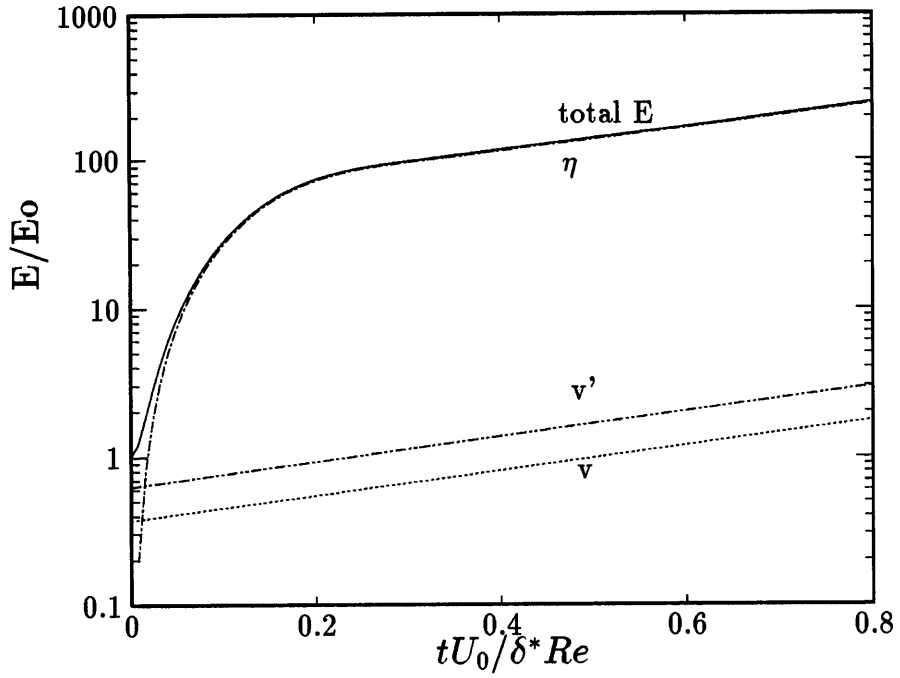

Figure 4-4: Temporal evolution of the total energy and its components with zero initial vertical vorticity, unstable mode. $\psi = 45^0, H = 0.3, Re = 500, \alpha = 0.1, \beta = 0.4$. The vorticity component grows exponentially at the same rate as the velocity.

energy decays exponentially while the vertical vorticity energy and the total energy are growing. On a linear scale, it can be seen that the vorticity grows linearly in time. As the homogeneous solution of the Squire equation drops out, it leaves only the particular solution, which has the same decay rate as the velocity component. In this case, the energy growth reached a maximum of about 25 times the initial energy. The energy growth obtained can be nearly thousandfold or just one, where the vorticity growth is so small that there is no discernible total energy growth.

The three-dimensional disturbance corresponding to a growing mode share some characteristics with those that decay. Because the velocity component grows, the vorticity part grows as well, so that there is never a 'maximum energy growth'. Instead, the initial growth rate decreases until the exponential growth rate of the vorticity component matches that of the velocity component. As in the case where the velocity decays, this is due to the homogeneous part dropping out of the solution, leaving only the particular solution associated with the vertical velocity.

The ratio of the energy component of the vorticity and velocity remains constant

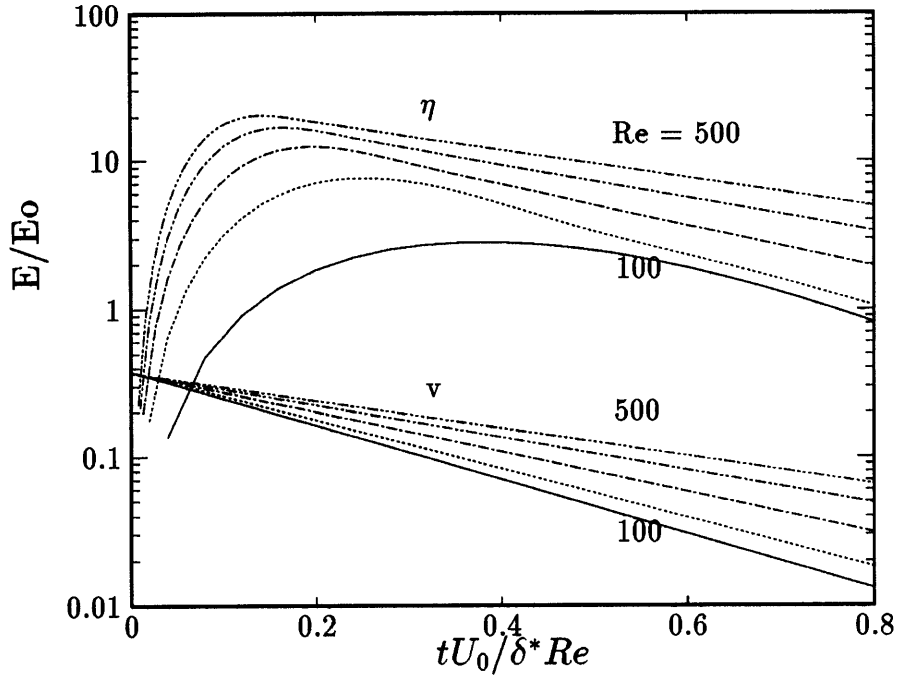

Figure 4-5: Vorticity and velocity energy evolution for various Reynolds numbers. $\psi = 45^0, H = 0.3, \alpha = 0.2, \beta = 0.25$. The initial growth rate is smaller for lower Re.

in figure 4-2, which is about 50 times the energy of the vertical velocity. Examination of the ratio for the same energy components in figure 4-3 where they are all uniformly decaying, shows that this ratio is exactly the same. If we can obtain the eigenfunction for velocity and vorticity of the least damped mode initially, the amplitude ratio of energy components can be determined without going through the time integration.

4.3 Evolution of the energy and its components

In this section, we will examine the temporal evolution of the energy and its components and find its dependence on various parameters. Figure 4-5 shows the evolution of various modes for different Reynolds numbers. The long time exponential decay rate appears proportional to $\mathcal{O}(Re^{-1})$. The initial vorticity energy growth rate is proportional to $\mathcal{O}(Re)$, while the ratio of the vorticity energy to velocity energy is similar for different Reynolds number. It should be noted that if we use the normal time scale t instead of t/Re, we see that the initial growth rate is nearly independent of the Reynolds number.

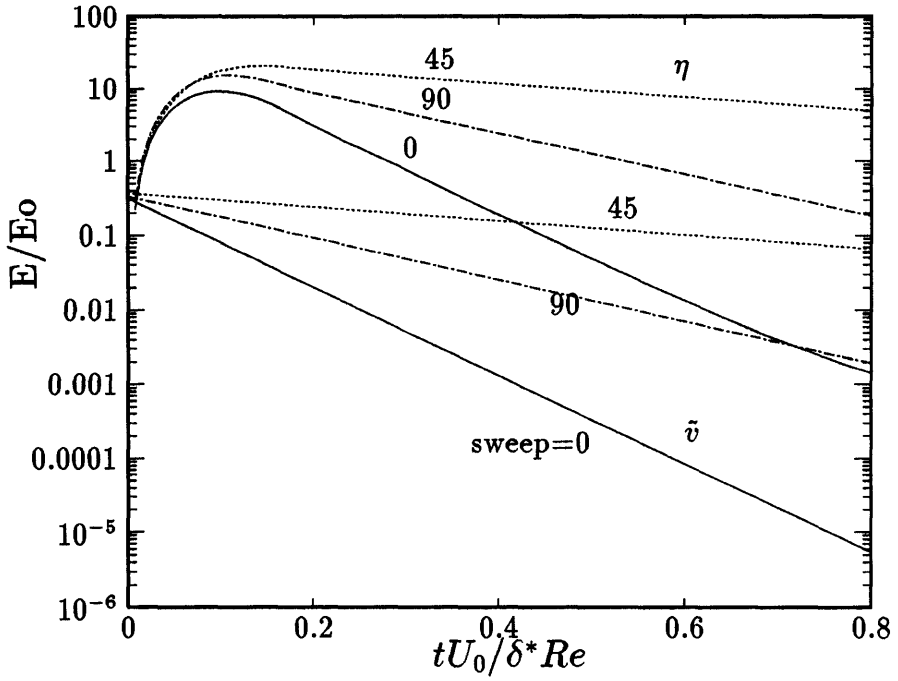

Figure 4-6: Temporal evolution of the velocity and vorticity energy for various ψ. $H = 0.3, Re = 500, \alpha = 0.2, \beta = 0.4$. The maximum depend only on the decay rate.

Examination of the energy growth for various values of H and ψ also shows that, for given α, β, and Reynolds number, the only significant difference is the long-time decay rate. The ratio of the vertical vorticity energy to the vertical velocity energy is of the same order, being only slightly smaller for waves that decay at a slower rate. The initial linear growth rate of the vertical vorticity energy is nearly identical as well. This result is illustrated in figure 4-6, where the mode with $\psi = 45^0$ has the largest growth. We can see that the initial linear growth remains nearly the same for three angles. The difference in energy growth obtained is only due to the difference in decay rates. Examination of energy evolution for flow with different H will give similar results, where only the decay rate shows significant difference.

Following conclusions can be drawn from examination of the temporal evolution of the energy for various flows. We find that the initial growth rate is apparently dependent only on α, and β. Taylor expansion of the solution of the Squire equation show that this is proportional to $i(\beta U' - \alpha W')$. However, since the energy is an integrated quantity, small variation in the mean flow profile does not vary the growth

rate of the vorticity energy greatly. Therefore, the initial growth rate of the vorticity depends mostly on α and β, and weakly on H, ψ, and the Reynolds number. Since the U' component is larger than the W' component, the effect of β will greater, and for most flows, the growth rate is $\mathcal{O}(\beta)$. The ratio of the vorticity energy to velocity energy can be obtained from the eigenfunctions used as initial conditions. While there is no empirical relation for this value, examination of various modes show that it is strongly dependent on α and β, and only weakly on H, ψ, and the Reynolds number. This ratio change from $\mathcal{O}(1)$ to $\mathcal{O}(\beta^2)$ as α increases from 0. It also seem to be $\mathcal{O}(\alpha^{-1})$. Unlike the previous two values, the decay rate of the energy is strongly dependent on the mean flow profile. Linear stability theory shows that even small variation in the mean flow profile can affect the stability of the flow. It is strongly dependent on all five parameters, α, β, H, ψ, and Re. Due to the sensitivity of the decay rate to the mean flow profile, no empirical relation can be given except those previously given for the Reynolds number.

4.4 Maximum energy growth

The temporal evolution of various modes have been examined in the previous section. In this section, the relationship of the maximum energy growth and α, β, H, ψ, and the Reynolds number will be examined. The values for $\alpha = 0$ have not been been calculated, since the eigenfunctions of the least damped mode for low value of α could not be obtained accurately for most cases due to numerical difficulties.

Figure 4-7 shows the maximum E/E_0 for the Blasius boundary layer for a range of α and β. Each line represents the maximum growth obtained by a certain value of α for various values of β. Since there is no crossflow, the result is symmetric about $\beta = 0$. We can see that as α decreases, the maximum growth becomes larger. For low α of 0.1 to 0.3, the maximum energy growth is gained for waves of $\beta = \pm 0.6$ to ± 0.7. For higher α, the maximum is obtained at β of more than 1 or less than -1.

Let us examine how a pair of Fourier modes with the same α, but with β of opposite sign will behave when the mean flow has a Falkner-Skan-Cooke velocity

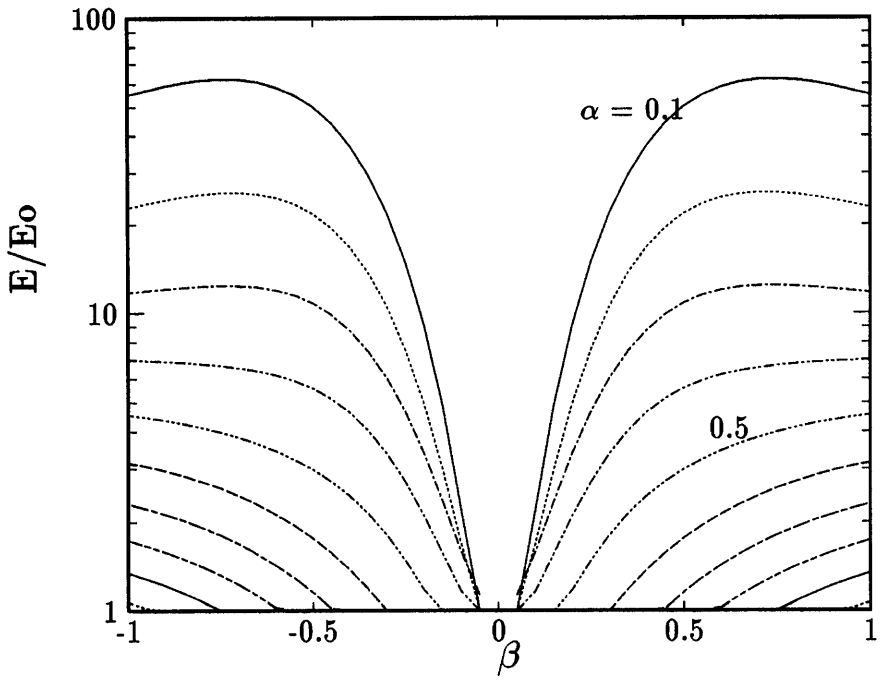

Figure 4-7: Maximum E/Eo for three-dimensional disturbance in Blasius boundary layer flow. $Re = 500$. Greater energy growth is obtained for lower α.

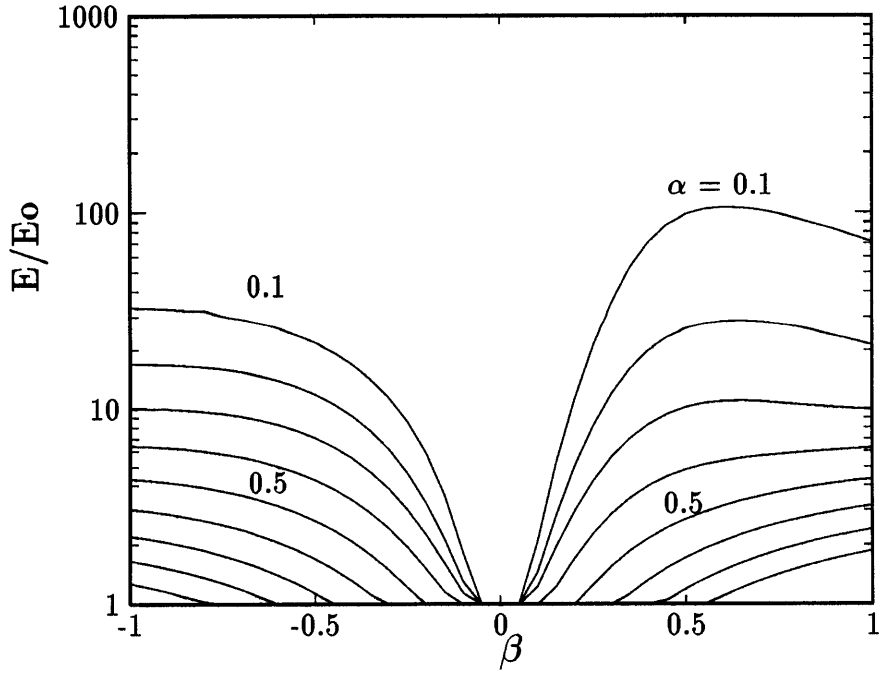

Figure 4-8: Maximum E/Eo obtained for various α plotted against β. $\psi = 45^0, H = 0.2, Re = 500$. Positive β gives larger growth; negative β gives smaller growth.

profile. We know from the linear stability theory for three-dimensional boundary layers that a wave that goes in the same direction as the crossflow is more stable, while those with the same α, but β of an opposite sign will be less stable. This result is shown in figure 4-8, where the value of $H = 0.2$ is used so that none of the modes are unstable. This figure shows the asymmetry due to the existence of a crossflow. The combination of positive α and positive β, which is less stable than positive α and negative β, has a larger maximum energy growth. Largest energy growth is obtained for $\alpha = 0.1$ with the maximum obtained for $\beta = 0.6$ when β is positive and at $\beta < -1$ when β is negative. In addition, since the forcing term of the Squire equation becomes smaller as β approaches 0, the transient growth also becomes small for smaller β. When $\beta = 0$, the forcing term has only the W' part, which is very small compared to the U' part, resulting in a minor growth of the vertical vorticity so that the energy growth does not exceed 1. However, for a boundary layer with larger crossflow, this $\alpha W'$ component can become large enough so that the energy growth can exceed 1 even when $\beta = 0$.

As the crossflow becomes larger due to the increase of H or ψ approaching 45^0, the asymmetry will increase. The stable waves will become more stable and decay faster, but the less stable waves will become even less stable and decay slower. We know that the initial linear growth rate and the amplitude ratio of the vorticity energy and velocity energy will remain similar so that the difference in the decay rate will determine the maximum energy growth obtained. When the crossflow is large enough, modes with low α will become unstable and exhibit growth. If the velocity profile with $H = 0.3$ is used, where some modes with $\alpha = 0.1$ and positive β are unstable, the energy will grow to infinity.

It has been shown that for $\alpha = 0$ mode in Poiseuille flow, the maximum vorticity energy obtained is $\mathcal{O}(Re^2)$, and the time that this is obtained is $\mathcal{O}(Re)$. Since the modes for $\alpha = 0$ were not obtained, this cannot be verified for boundary layer flow. However, for $\alpha \neq 0$, as α is increased, the maximum energy growth obtained shifts from $\mathcal{O}(Re^2)$ to $\mathcal{O}(Re)$. Figure 4-9 shows the relationship between the maximum energy obtainable for β and Re when $\alpha = 0.1$. It can be seen that they are somewhat

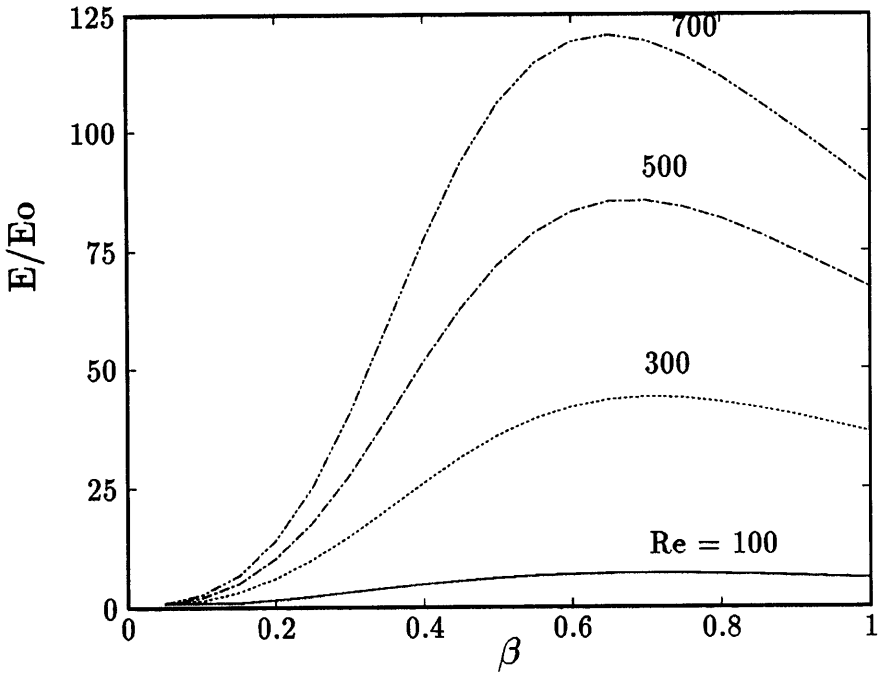

Figure 4-9: Maximum E/Eo obtained for various Re plotted against β. $\psi = 45^0, H = 0.1, \alpha = 0.1$. The maximum energy growth is slightly less than $\mathcal{O}(Re^2)$.

less than $\mathcal{O}(Re^2)$. As α is reduced, this relationship asymptotes toward $\mathcal{O}(Re)$. We can also see that the maximum energy growth is obtained for $\beta = 0.6$ for different values of Re.

The maximum E/Eo for various H are shown in figure 4-10 for $\psi = 45^0$ and $\alpha = 0.1$. The time evolution of the same mode for different H was discussed in the previous section. For a given value of α and β, we can expect a similar initial growth rate and ratio of the vorticity energy to the velocity energy. Here, we can see that in addition to causing the growth to increase for positive β and to decrease for negative β, it also shifts the β that gives the maximum growth. For positive β, this shifts from 0.6 to 0.4, and for negative β, it shifts to a more negative value of β. This shift is due to instability of the vertical velocity part due to the crossflow. For the Blasius boundary layer, the least stable wave is at $\beta = 0$, but the largest energy growth is obtained for $\beta = 0.6$ from the optimal combination of the energy ratio, initial growth rate, and decay rate. However, as H increases, decay rate of waves at $\beta = 0.4$ become lower because of crossflow instability, so that the combination of the energy ratio and

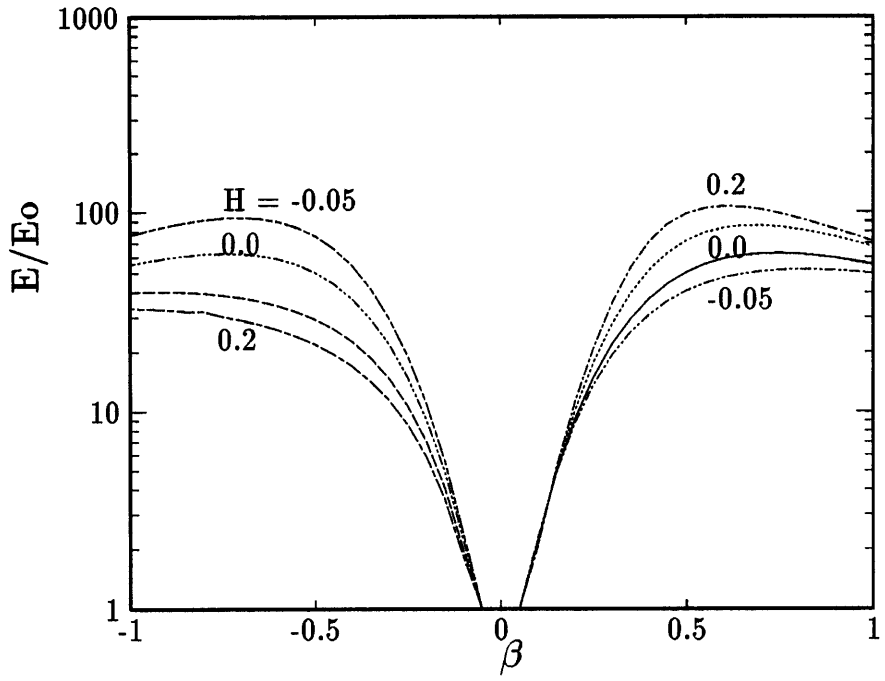

Figure 4-10: Maximum E/Eo obtained for various H plotted against β. $\psi = 45^0, Re = 500, \alpha = 0.1$.

the initial growth rate will give these waves large energy growth. This causes the shift in the β that gives the largest energy growth. If H is increased even more, these waves will become unstable, showing infinite growth.

For negative H, the largest energy growth is obtained for negative β, but otherwise, it remains identical to the cases where $H > 0$, showing similar increases of the asymmetry as H decreases. However, the waves that become unstable first are those near $\alpha = 0.3$ and $\beta = 0$, due to the streamwise instability. Therefore, lower β will exhibit larger energy growth than when $H > 0$.

Figure 4-11 shows the relationship of the maximum energy growth and the sweep angle for $\alpha = 0.1$. The results for $\psi = 0^0$ and $\psi = 90^0$ are symmetric, while the results for other ψ are asymmetric, with largest asymmetry occurring for $\psi = 45^0$. We can also see that the β that gives the maximum energy growth shifts from 0.7 to 0.5 as ψ increases and then back to 0.7 again. For negative β, the β that gives the maximum growth shifts from -0.7 to a lower value, then comes back up to -0.7. This shift in the β for the largest growth can also be attributed to the effect of the

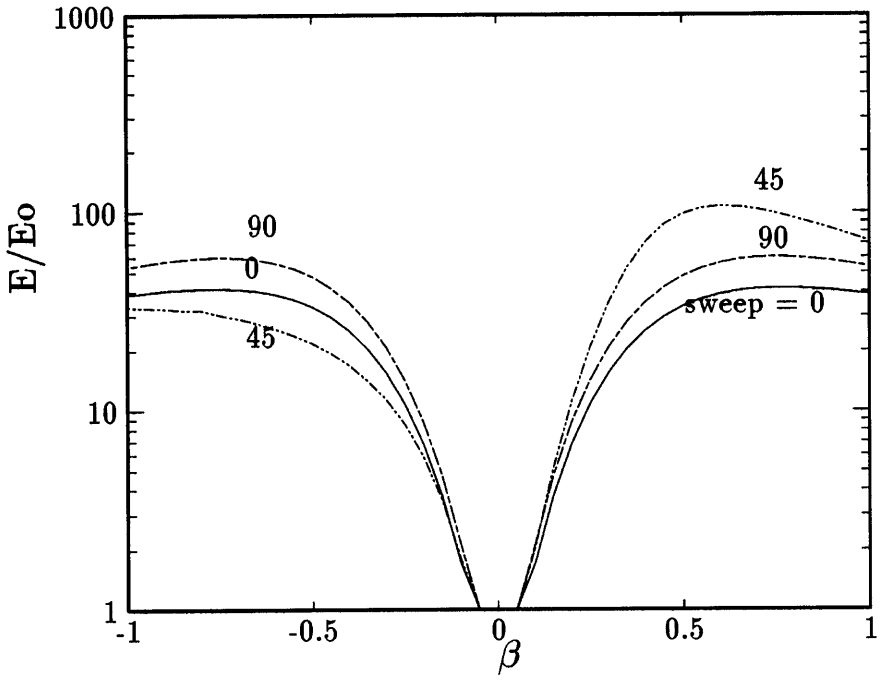

Figure 4-11: Maximum E/Eo obtained for various ψ plotted against β. $H = 0.3, Re = 500, \alpha = 0.1$. For positive β, the result rises from the lowest line up to the highest line where $\psi = 45^0$ and then descends to the line of $\psi = 90^0$. For negative β, it is the opposite.

crossflow instability on the decay rate.

We can conclude that the maximum energy growth where ψ and H are varied depends only on the decay rate of the eigenfunction. Therefore, the linear stability of the flow determines the decay rate and consequently the maximum energy growth obtained when the initial growth rate and the amplitude ratio of the energy is similar.

4.5 Prediction of the maximum energy growth

It is possible to predict of the maximum energy growth from the analysis of the temporal evolution using the conclusions drawn in Section 4.3. The necessary parameters are the exponential decay rate, the ratio of the vorticity energy to the velocity energy, and the initial linear growth rate of the vorticity. The intersection of two curves, where one represent the energy of the exponentially decaying vorticity of the complete mode, and the other the initial linear growth of the vorticity, will give the

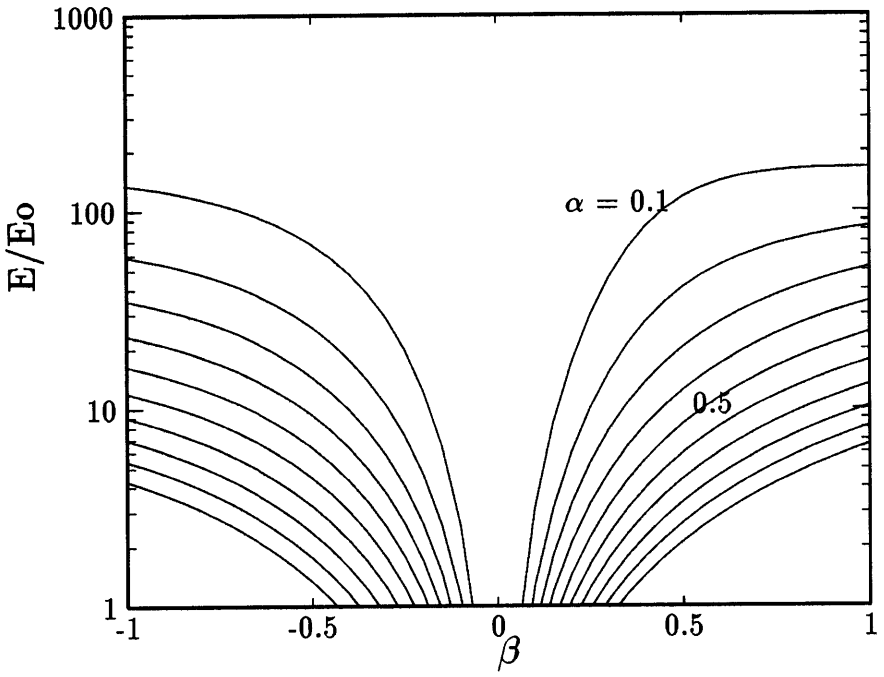

Figure 4-12: Maximum E/Eo predicted for various α plotted against β. $\psi = 45^0, H = 0.2, Re = 500$.

approximate maximum energy growth and time it is obtained.

The initial linear growth of the vorticity is proportional to $i(\beta U' - \alpha W')$, resulting in the following equation:

$$\tilde{\eta} = i(\beta U' - \alpha W')\tilde{v}_0 t, \tag{4.1}$$

while the vorticity energy is given by

$$E_{\tilde{\eta}} = \int_0^\infty \frac{1}{k^2} |(\beta U' - \alpha W')\tilde{v}_0 t|^2 dy. \tag{4.2}$$

This value has to match the energy of the exponentially decaying complete mode, which is given by the following equation:

$$E_\eta = (\int_0^\infty \frac{1}{k^2} |\eta_0 e^{\alpha C_i t}|^2 dy). \tag{4.3}$$

The coefficients for this equation can be obtained by solving the Orr-Sommerfeld and Squire equation as eigenvalue problems and obtaining the decay rate and the ratio of the vorticity energy to the velocity energy.

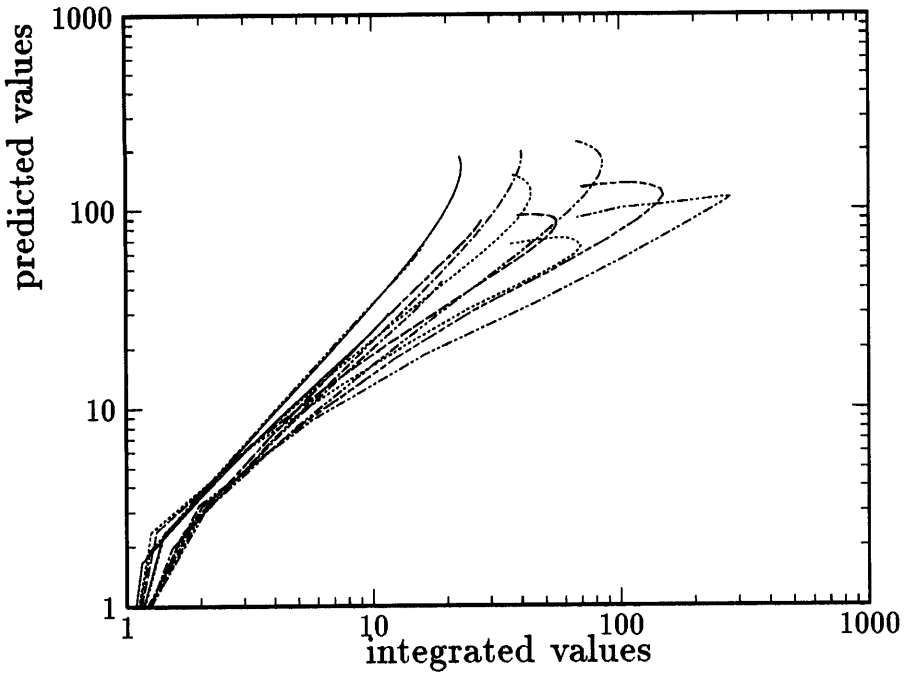

Figure 4-13: Correlation of values of maximum E/Eo obtained from prediction and numerical integration for various β modes. $\alpha = 0.1, Re = 300$ and 500, $H = 0.1$, 0.3, and 0.5.

The time t when these two curves intersect is obtained by solving the equation using Newton's method. The result is entered into (4.2), giving the predicted maximum energy. This prediction will give higher values for modes that have strong decay rate, while for those modes with weak decay rates, the result will be more accurate. The results are shown in figure 4-12 for the case of $Re = 500$, $H = 0.2$, and $\psi = 45^0$. If the necessary adjustment for those modes with higher decay rate is made, the results will match quite well with the results in figure 4-8.

In order to examine the correlation between the predicted values and numerically integrated values, the matching is plotted in figure 4-13. The x-axis is the integrated values, and the y-axis shows the predicted values. Prediction give values that are about two or three times the actual values for smaller values of β, and becoming more varied for higher β. While the method of prediction is very crude, we can see that it can give good estimate of the maximum energy that can be obtained for a particular mode.

4.6 Continuous spectrum modes and arbitrary initial conditions

Studies of the eigenvalue spectrum for a bounded viscous flow such as the Poiseuille flow have shown that they have only discrete spectrum of eigenmodes. However, Gustavsson [8] has shown that in addition to the discrete modes, modes in the continuous spectrum are also required for unbounded flows in order to describe an arbitrary disturbance. Grosch and Salwen [7] have shown that this continuous spectrum has a finite energy and that each mode is sinusoidal in form outside the boundary layer. They have also shown that for a flat plate boundary layer, this continuous spectrum forms a line at $C_r = 1$.

The numerical simulation also captures the modes at $C_r = 1$. However, these modes are not exactly a physical phenomenon but a mode required by the finite numerical approximation. Like the continuous spectrum, these modes are bounded and do not decay as y increases. However, they are not truly sinusoidal and depend strongly on the location of the Chebyshev collocation points in y. The nature and behavior of this mode resembles that of the continuous spectrum, but care is needed to interpret the results obtained.

Even though there is no discrete mode for the two-dimensional boundary layer at $\alpha = 0$ that can be used as an initial condition, it is possible to give an arbitrary disturbance and observe its evolution. The initial vertical velocity was given by the following equation while the initial vertical vorticity was set to zero:

$$v(y) = y^2 e^{y^{-2}}. \tag{4.4}$$

Figure 4-14 shows the time evolution of the total energy. Figure 4-15 shows the vertical velocity profile for $\beta = 0.25$ at time $tU_0/\delta^* = 0, 200, 400$, and 600. The initial velocity profile decays while a velocity profile centered around $y = 4\delta^*$ dominates the solution, which is outside the boundary layer. The phase speed, C_r, which is nearly equal to 1, also indicates that this component is composed of continuous spectrum

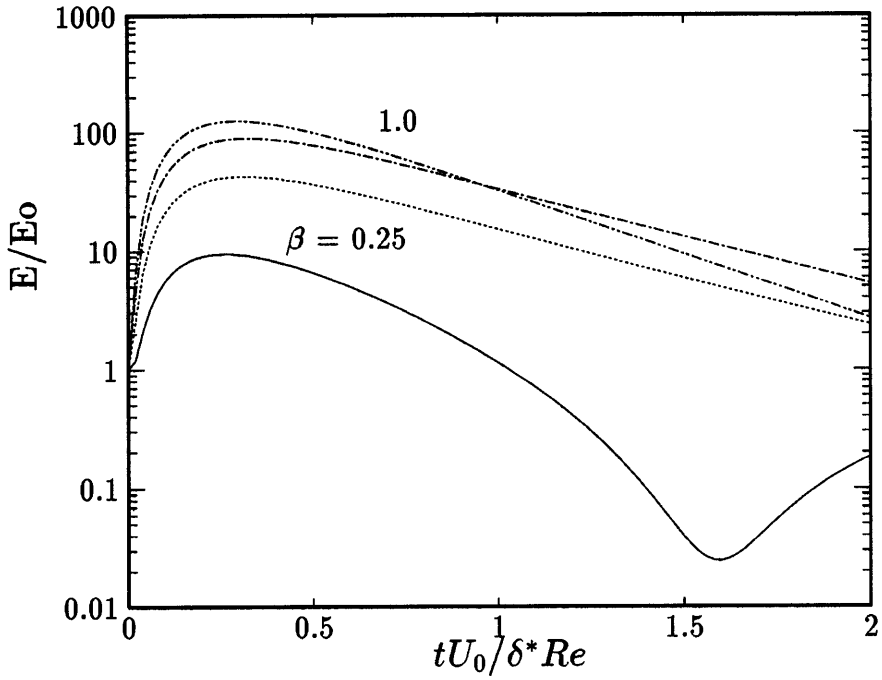

Figure 4-14: Energy evolution for an arbitrary initial condition for $\alpha = 0$ mode in a Blasius boundary layer flow. $Re = 500$, and $\beta = 0.25$-1.00

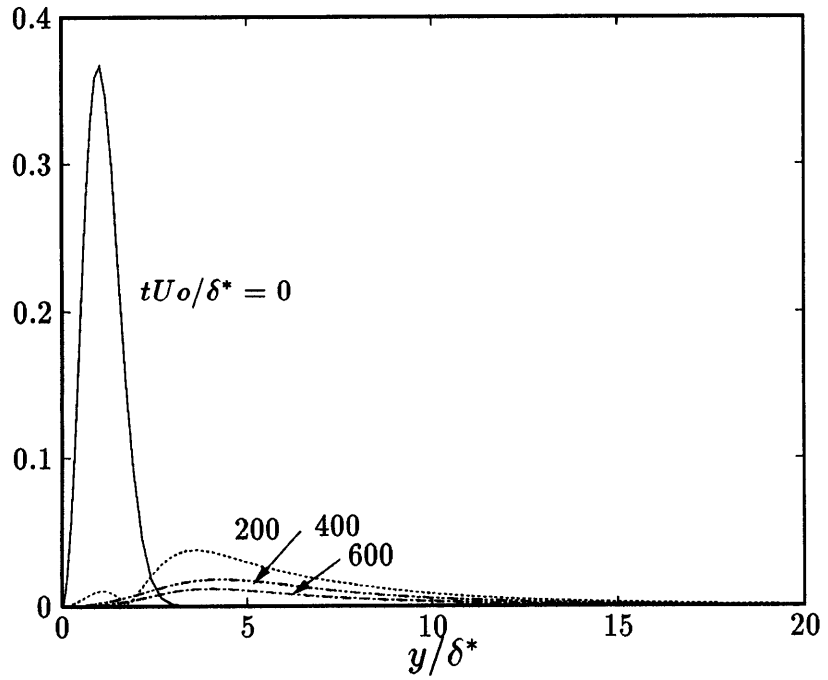

Figure 4-15: Vertical velocity profile for $\beta = 0.25$ at $tU_0/\delta^* = 0, 200, 400$, and 600.

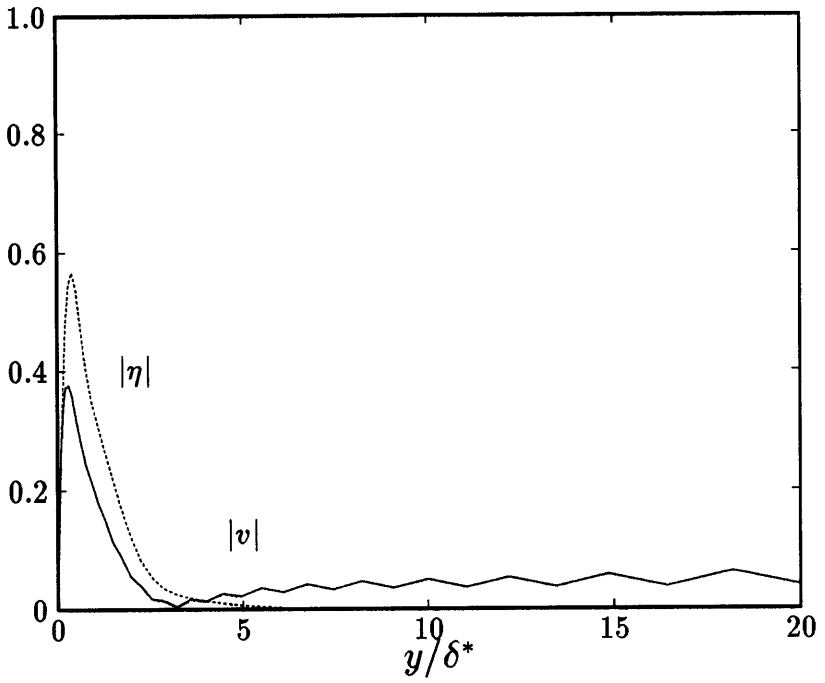

Figure 4-16: Eigenfunction of a least damped continuous mode. $\psi = 45^0, H = 0.3, Re = 500, \alpha = 0.2, \beta = 0.4$. The vertical velocity profile extend outside the boundary layer.

modes. We can assume that this mode is a combination of non-orthogonal continuous spectrum modes. The process of energy growth for these initial conditions is similar to that of discrete modes. We can see that even though they are arbitrarily given, they give results greater than any of the results for discrete modes in a Blasius flow, supporting the prediction that the mode with $\alpha \simeq 0$ will have the greatest energy growth.

Figure 4-16 shows the profile of a least-damped 'continuous spectrum' mode for a three-dimensional boundary layer. $|\tilde{v}|$ resembles an actual continuous spectrum mode, which is sinusoidal in the free stream. However, each peak or valley corresponds to a Chebyshev collocation point. The corresponding vertical vorticity eigenfunction is zero outside the boundary layer since the forcing term of the Squire equation goes to zero as the mean shear goes to zero. The calculation of energy showed that despite the fact that the vertical vorticity has larger maximum amplitude, the vertical velocity has more energy because of its structure extending outside the boundary layer to infinity.

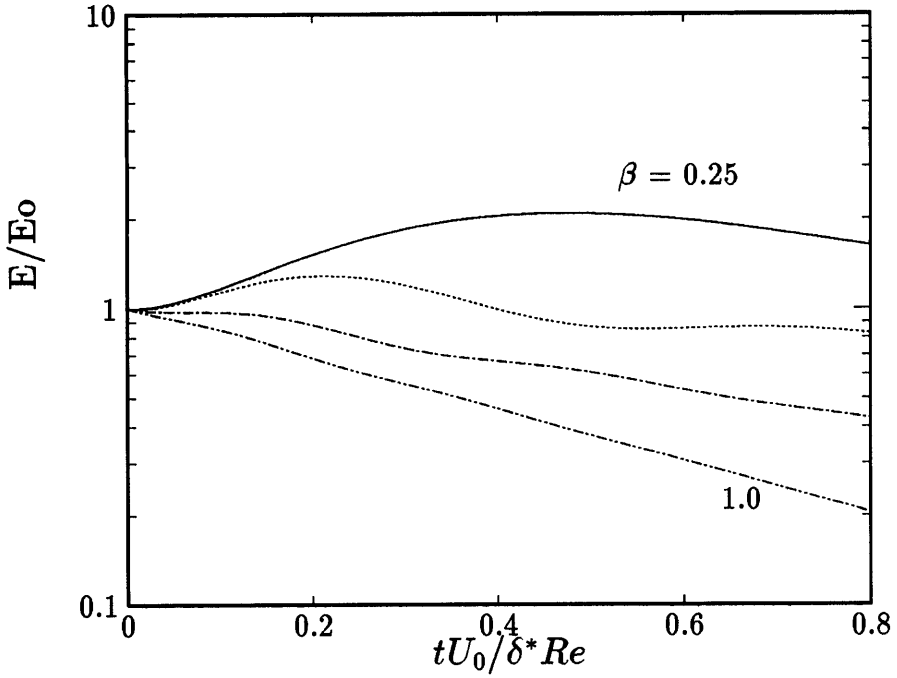

Figure 4-17: Energy evolution with continuous spectrum modes as initial conditions for $\alpha = 0$ modes. $Re = 500$, $H = 0.3$, $\psi = 45^0$, and $\beta = 0.25$-1.00

The temporal evolution of v using this mode as the initial condition, is given in figure 4-17. Despite the fact that this is the least damped mode for $\alpha = 0$, the maximum energy growth obtained is only twice the initial energy for $\beta = 0.25$. This small energy growth results from the fact the vertical velocity component having a profile extending to infinity while the vorticity component profile is limited within the boundary layer. Therefore, the ratio of the velocity energy and the vorticity energy is small compared to the discrete modes. In addition, we can see that the modes that were calculated were not a single mode, but was actually composed of multiple modes. This can be seen in the beating phenomenon observed for modes with higher β. The same phenomenon was observed and analyzed by O'Sullivan and Breuer [16] in their examination of the transient growth in pipe flow. This phenomenon is due to multiple continuous spectrum modes decaying at nearly the same rate, but with slightly different phase speed.

Unlike the two-dimensional boundary layer, where there is no discrete spectrum when $\alpha = 0$, a three-dimensional boundary layer with non-zero W does have discrete

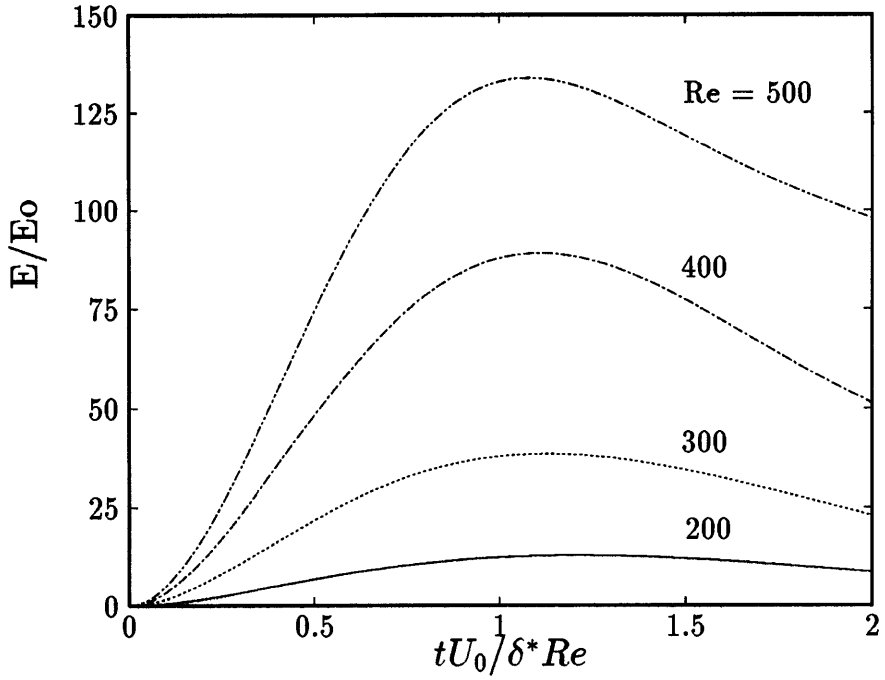

Figure 4-18: Vorticity energy evolution for various Reynolds number. $\psi = 45^0, H = 0.3, \alpha = 0, \beta = 0.25$. The maximum energy and $t_{\max}$ is $\mathcal{O}(Re)$.

modes. This allows examination of cases where $\alpha = 0$. However, due to numerical difficulties in the calculation, this mode was very difficult to calculate. Therefore, an arbitrary initial condition was used initially, and marched forward in time until all other modes decayed away. The final velocity profile was then used as the initial condition for case of $\alpha = 0$. This result is shown in figure 4-18. The results show that the maximum energy amplitude is $\mathcal{O}(Re^2)$ and the time that it is obtained is $\mathcal{O}(Re)$. This result matches quite well with the results for Poiseuille flow by Henningson [10] and Gustavsson [9]. Unfortunately, this mode cannot be proven to be the least-damped discrete mode, and is presented here only for future analysis.

Chapter 5

Localized Disturbances

5.1 Details

The computational domain was a box with length of $200\delta^*$ in the streamwise direction and width of $50\delta^*$ in the crossflow direction. The numbers of the discrete points in the x- and z-direction were both set to 32. A Falkner-Skan-Cooke boundary layer with $H = 0.5$ and $\psi = 45^0$ which has a maximum crossflow velocity of $-0.08U_0$ was used as the mean flow, while the Reynolds number was set to 950.

Figure 5-1 shows the two pairs of counter-rotating vortices used as the initial condition. This disturbance, first used by Russell and Landahl [20], is derived from the following two-dimensional stream function:

$$u = 0, \tag{5.1}$$

$$v = -\frac{\partial \Psi}{\partial z}, \tag{5.2}$$

$$w = \frac{\partial \Psi}{\partial y}, \tag{5.3}$$

where

$$\Psi = \bar{x}\bar{z}\bar{y}^2 \mathrm{e}^{-\bar{x}^2-\bar{y}^2-\bar{z}^2}, \tag{5.4}$$

and $\bar{x}$, $\bar{y}$, and $\bar{z}$ are Cartesian coordinates scaled by the characteristic lengths l_x, l_y,

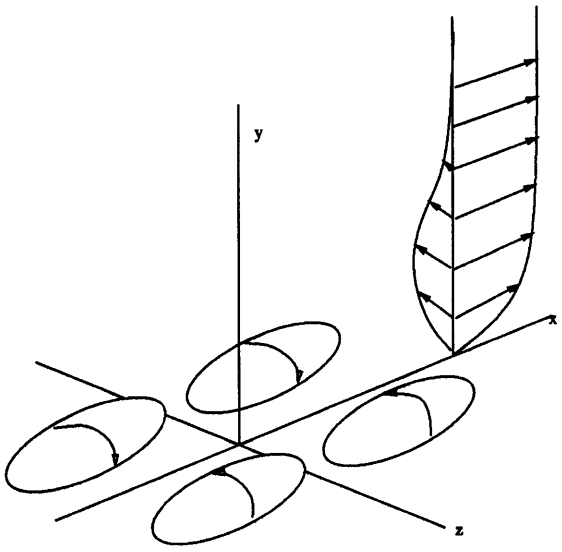

Figure 5-1: Schematic of the two pairs of counter-rotating vortices used as the initial perturbation

and l_z:

$$\bar{x} = x/l_x, \tag{5.5}$$

$$\bar{y} = y/l_y, \tag{5.6}$$

$$\bar{z} = z/l_z. \tag{5.7}$$

The scale lengths were set to $l_x = 5\delta^*$, $l_y = 1.2\delta^*$, and $l_z = 6\delta^*$ so that comparisons could be made with the results of Breuer and Haritonidis [2].

Due to the nature of the initial condition, the initial vertical vorticity is not zero. However, it is sufficiently small so that we can still expect a large growth of the vertical vorticity component. Also, this initial condition does not excite the $\alpha = 0$ mode, which would give even larger transient growth.

5.2 Results

Figures 5-2, 5-3, 5-4, and 5-5 show the evolution of the localized disturbance. The flow is from left to right, and the boundary layer thickness is approximately $3\delta^*$. The contour spacing for the vertical velocity perturbation is 0.125 of the maximum

initial vertical velocity perturbation, while the spacing for the horizontal velocity perturbation is 1.25 of the maximum initial velocity perturbation. The solid lines represent the contours for the positive values; the dotted lines represent the contours for the negative.

If we examine the vertical velocity perturbation in figure 5-2, we can see that it is quite similar to the results by Breuer and Haritonidis. They show that the structure of the vertical velocity perturbation extends out of the boundary layer and is apparently exponentially decaying in the free stream. The structure remains coherent, while the perturbation amplitude is decaying slowly in time.

Figure 5-3 shows the vertical velocity perturbation in the $y = 1$ plane, with the vertical perturbation decaying in time. However, unlike the Blasius boundary layer case, the perturbation loses its symmetry due to the crossflow. This can be understood from linear stability theory for three-dimensional boundary layers. The decay rate for a wave with the same α and a positive β is smaller than its counterpart with negative β. Therefore, the waves in the positive z-direction decay slower than in the negative direction. This appears in figure 5-3 as streak-like regions of positive and negative vertical velocity perturbation.

The horizontal velocity perturbation in figure 5-4 resembles the result for the Blasius boundary layer as well. The inclined shear layer resulting from the mean shear in the streamwise direction is formed, which is then stretched and intensified. The effect of the crossflow is not obvious, since the mean streamwise velocity U dominates the behavior of the solution in the streamwise direction.

However, the effect of the crossflow on the horizontal velocity perturbation is evident in figure 5-5. The horizontal velocity contour loses its symmetry because the perturbation is advected in the direction of the crossflow as well as in the streamwise direction. Since the mean crossflow has its maximum near $y/\delta^* = 1$, the perturbation in that vicinity will be advected in the crossflow direction more than the fluid near the wall or outside the boundary layer. As the slower moving fluid near the wall is lifted up, its displacement in the negative z direction is less than that of the faster fluid. The two regions of low speed flow remain separate for the Blasius boundary

layer but in this case combine and form an elongated region of low speed flow. Similar phenomenon occurs for the high speed region as well.

These streamwise streaks were observed by Henningson for a Poiseuille flow when he used a similar pair of counter-rotating vortices set at a 30-degree angle to the mean flow. This kind of feature will cause the mean streamwise velocity profile to have spanwise variation. The initial condition used by Henningson excited the $\alpha = 0$ mode, which has the maximum transient energy growth. This streak-like feature is an important part of the non-linear interactions in the breakdown of the laminar flow and is also often observed in turbulent flows. In this case, even though no $\alpha = 0$ mode was excited initially, streak-like formations appeared as well, which can lead to nonlinear interactions. However, unlike the other cases, these formations will not remain fixed in z, but will 'drift' in the crossflow direction.

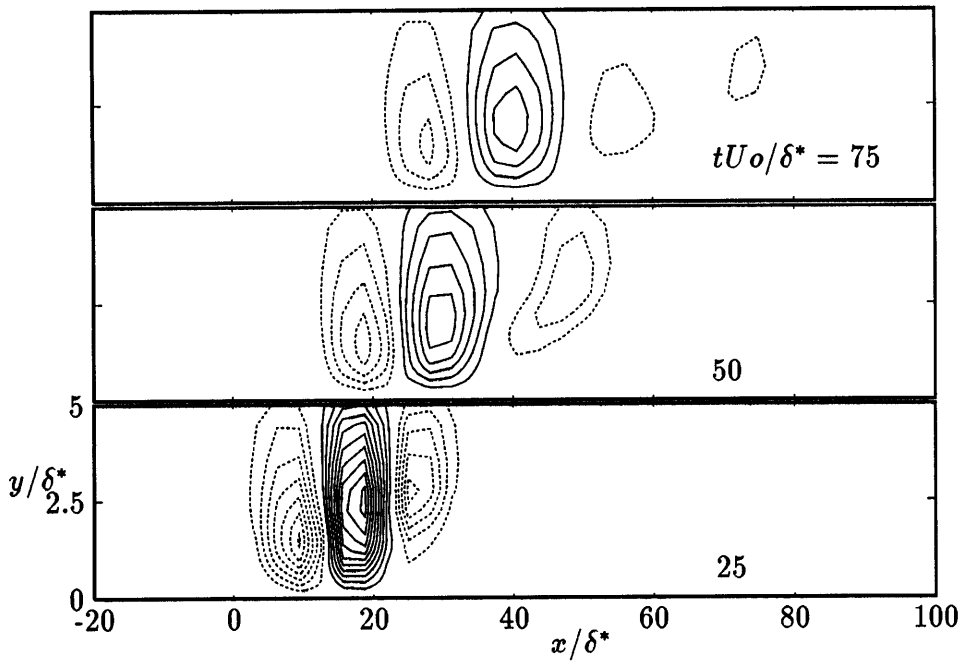

Figure 5-2: Contours of the vertical velocity perturbation in the (x, y) plane at $z = 0$. The perturbation extends outside the boundary layer and decays slowly. Contour spacing is 0.125 of the maximum initial vertical perturbation. The solid lines represent the positive contours, and the dotted lines represent the negative contours.

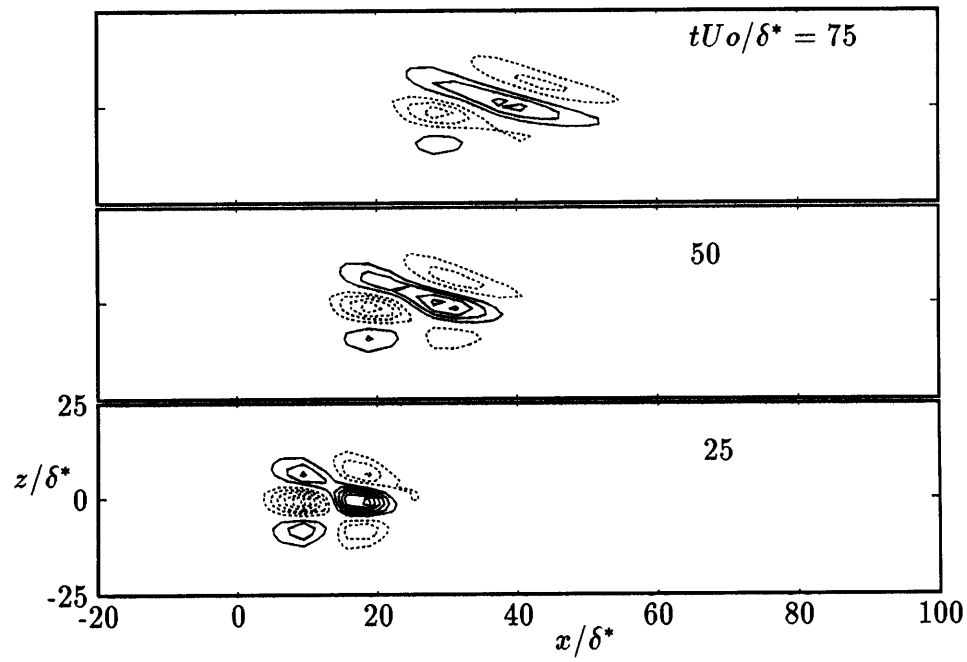

Figure 5-3: Contours of the vertical velocity perturbation in the (x, z) plane at $y/\delta^* = 1$. Contour spacing is 0.125 of the maximum initial vertical perturbation.

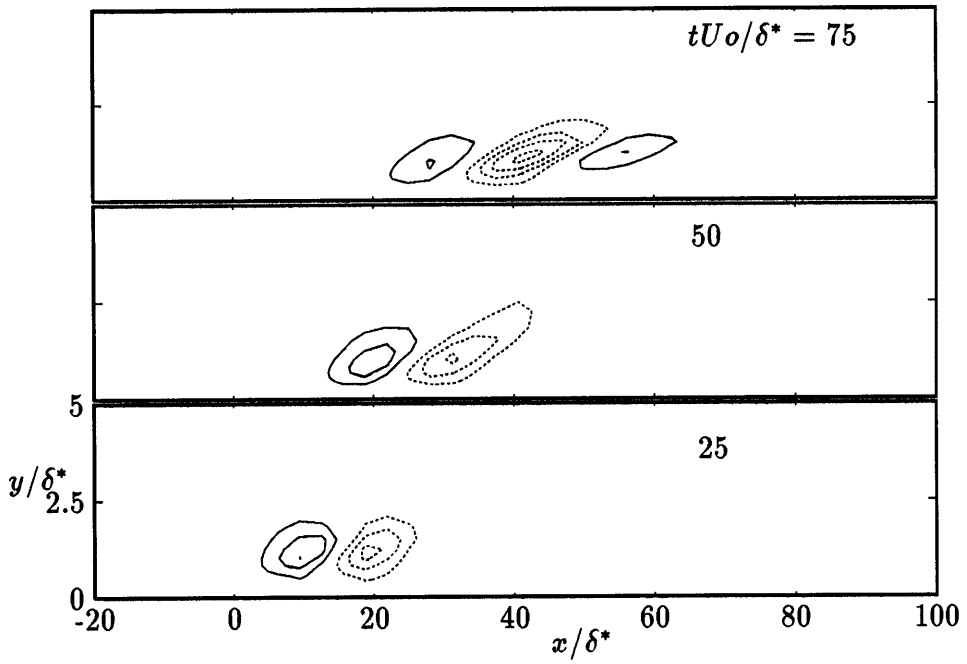

Figure 5-4: Contours of the streamwise velocity perturbation in the (x, y) plane at $z = 0$. Formation of the inclined shear layer. Contour spacing is 1.25 of the maximum initial vertical perturbation.

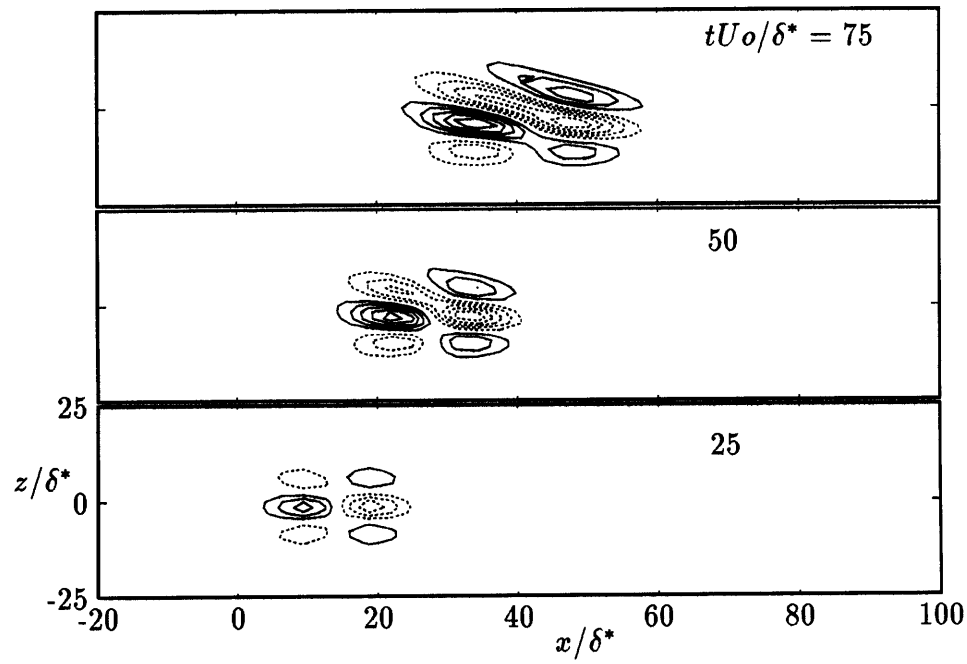

Figure 5-5: Contours of the streamwise velocity perturbation in the (x, z) plane at $y/\delta^* = 1$. Streaks of high and low speed region. Contour spacing is 1.25 of the maximum initial vertical perturbation.

Chapter 6

Concluding Remarks

Traditional study of the transition have assumed that only the long-term behavior of unstable T-S waves are important in determining transition and that the transient behavior can be disregarded. However, examination of the three-dimensional nature of the evolution of a disturbance have shown that transient energy growth of two or three orders of magnitude can occur even when linear theory predicts decay. This quick and large energy growth can immediately lead to non-linear interactions and subsequent breakdown to turbulent flow. In order to completely understand the mechanism of transition, this phenomenon can not be disregarded, making it necessary to examine both the transient and the long-term evolution of disturbances. In addition, unlike the traditional stability theory where the streamwise T-S waves are most important, we find that these waves actually has the least energy growth, while waves that creates the most energy are those in the crossflow or the spanwise direction. This requires us to examine the mechanism of transition from a totally different angle.

We have shown that substantial transient growth is possible in boundary layer flows and that it has a mechanism identical to that of the Poiseuille flow. Like the transient growth in channel flow, it is strongly dependent on initial conditions, attaining the largest energy growth when the initial vertical vorticity is equal to zero. In addition, largest energy growth is obtained when α is equal to or close to zero, and is $\mathcal{O}(Re^2)$.

However, unlike the Poiseuille flow which has discrete $\alpha = 0$ modes, there is no

discrete $\alpha = 0$ mode for the Blasius boundary layer, due to the fact that the flow is unbounded in the free stream. Since $\alpha = 0$ disturbance is composed entirely of continuous spectrum modes, this flow can not be examined using discrete modes. In addition, the numerical scheme is not suitable for examining the continuous spectrum modes since there is only a finite number of collocation points in the free stream. Even for three-dimensional flows, calculation of the $\alpha = 0$ mode is difficult since the discrete mode could not be obtained accurately. Therefore, direct comparison with results for Poiseuille flow was not possible. However, a rough estimate based on an arbitrary initial condition was given and showed good agreement with the expected results.

Examination of temporal evolution of various modes shows that the initial vorticity growth is nearly linear until it reaches a maximum and then decays or grows at the same rate as the velocity. The maximum energy growth depends mainly on three parameters; the initial growth rate of the vorticity, the ratio of the vorticity and velocity energy in the eigenfunction, and the exponential decay rate. It was possible to make predictions of the energy growth using the eigenmodes and the eigenfunctions of the least damped modes, which showed good agreement with calculated results.

The introduction of crossflow does not change the basic nature of the transient growth. For flow with small crossflow, the effect of crossflow is to change the decay rate of the flow and thus change the maximum energy growth obtained for a particular wave. However, unlike the Blasius boundary layer where the least stable wave and the wave that exhibit larger transient growth were completely separate, for three-dimensional flow with larger crossflow, the least stable wave which is in the crossflow direction is also the wave that causes the largest transient growth. This result in formation of streamwise streak-like regions of high- and low-speed flow, which intensifies as the disturbance evolves downstream. This can lead to the distortion of the mean flow, which is a feature commonly observed in transition on swept wings.

Examination of the transient energy growth can add greatly to understanding of transition, especially those due to three-dimensional disturbances such as a localized isolated imperfection on wing surface or surface roughness. In addition, we also see that they have strong resemblance to the flow structure of the secondary instability,

which is characterized by spanwise variation of the mean flow due to streamwise vortices. For two-dimensional flows, the streamwise vortices have been assumed to be secondary in nature, generated by non-linear interactions between the mean flow and various waves. However, we have shown that this streamwise streak-like phenomenon can occur linearly as primary mechanism with substantial energy amplification. While this thesis have concentrated on laminar flows, we can also compare and possibly extend the results to turbulent flows, where streamwise streaks-like regions of high and low velocity are observed.

The system of equations and the method for numerical integration presented should be adaptable to variety of cases. Some possibilities include examining the evolution of disturbance for different boundary conditions, mean flow profiles, and initial conditions. The boundary conditions for the wall can be changed to simulate suction, blowing, or different wall configurations, such as a wavy wall. The mean flow profile can be modified for other kinds of three-dimensional flow such as boundary layer on a rotating disk, or an arbitrary three-dimensional boundary layer flow. Since the transient growth is strongly dependent on the initial condition, use of such initial conditions such as the optimal perturbations obtained by Butler and Farrell [3] may provide additional insights into transition.

While results similar to other kinds of flow have been obtained (notably Henningson [10] and Gustavsson [9]), they remain incomplete due to the fact that the $\alpha = 0$ mode which is so important in the Poiseuille flow could not be examined exactly. This requires a better understanding of the continuous spectrum modes, which was not possible with the method used in this work. However, even the results for discrete modes with non-zero α show that this transient growth can be an important part of transition especially in three-dimensional boundary layers. While the understanding of the phenomenon of transition have come a long way from a century ago, it is clear that there is still very much more to be understood. In order to further understand this phenomenon, not only must we understand the behavior of the basic two-dimensional waves, but we must also examine and understand the transient and three-dimensional nature of disturbances in more details.

Appendix A

Details of Derivations

A.1 The Orr-Sommerfeld and the Squire equations

The non-dimensional linearized viscous three-dimensional equations of motion are:

$$u_t + Uu_x + U_y v + Wu_z = -p_x + \frac{1}{Re}\nabla^2 u, \tag{A.1}$$

$$v_t + Uv_x + Wv_z = -p_y + \frac{1}{Re}\nabla^2 v, \tag{A.2}$$

$$w_t + Uw_x + W_y v + Ww_z = -p_z + \frac{1}{Re}\nabla^2 w, \tag{A.3}$$

while the continuity requirement gives:

$$u_x + v_y + w_z = 0. \tag{A.4}$$

After taking the Fourier transform of all four equations in the x- and z-direction, we have:

$$[\frac{\partial}{\partial t} + i\alpha U + i\beta W - \frac{1}{Re}(\frac{\partial^2}{\partial y^2} - k^2)]\tilde{u} + U'\tilde{v} = -i\alpha\tilde{p}, \tag{A.5}$$

$$[\frac{\partial}{\partial t} + i\alpha U + i\beta W - \frac{1}{Re}(\frac{\partial^2}{\partial y^2} - k^2)]\tilde{v} = -\frac{\partial}{\partial y}\tilde{p}, \tag{A.6}$$

$$[\frac{\partial}{\partial t} + i\alpha U + i\beta W - \frac{1}{Re}(\frac{\partial^2}{\partial y^2} - k^2)]\tilde{w} + W'\tilde{v} = -i\beta\tilde{p}, \quad (A.7)$$

$$i\alpha\tilde{u} + \tilde{v}_y + i\beta\tilde{w} = 0, \quad (A.8)$$

where a tilde represents a transformed quality. α is the streamwise wave number, β the spanwise wave number and $k^2 = \alpha^2 + \beta^2$. From these equations, the transformed pressure is derived:

$$\tilde{p} = \frac{1}{k^2}[i(\alpha U' + \beta W')\tilde{v} - \{\frac{\partial}{\partial t} + i\alpha U + i\beta W - \frac{1}{Re}(\frac{\partial^2}{\partial y^2} - k^2)\}\tilde{v}_y]. \quad (A.9)$$

After taking the y-derivative of (A.9) and substituting into (A.6), we obtain:

$$[\frac{\partial}{\partial t} + i(\alpha U + \beta W)](\frac{\partial^2}{\partial y^2} - k^2)\tilde{v} - i(\alpha U'' + \beta W'')\tilde{v} - \frac{1}{Re}(\frac{\partial^2}{\partial y^2} - k^2)^2\tilde{v} = 0, \quad (A.10)$$

which is the Orr-Sommerfeld equation.

However, we would also like to observe the behavior of the horizontal velocities as well. These can be obtained as follows:

$$\begin{aligned}
&[\frac{\partial}{\partial t} + i(\alpha U + \beta W) - \frac{1}{Re}(\frac{\partial^2}{\partial y^2} - k^2)]\tilde{u} \\
&\quad = (\frac{\alpha\beta}{k^2}W' - \frac{\beta^2}{k^2}U')\tilde{v} + \frac{i\alpha}{k^2}[\frac{\partial}{\partial t} + i(\alpha U + \beta W) - \frac{1}{Re}(\frac{\partial^2}{\partial y^2} - k^2)]\tilde{v}_y, \quad (A.11) \\
&[\frac{\partial}{\partial t} + i(\alpha U + \beta W) - \frac{1}{Re}(\frac{\partial^2}{\partial y^2} - k^2)]\tilde{w} \\
&\quad = (\frac{\alpha\beta}{k^2}U' - \frac{\alpha^2}{k^2}W')\tilde{v} + \frac{i\beta}{k^2}[\frac{\partial}{\partial t} + i(\alpha U + \beta W) - \frac{1}{Re}(\frac{\partial^2}{\partial y^2} - k^2)]\tilde{v}_y. \quad (A.12)
\end{aligned}$$

We can simplify these equations by rotating the horizontal axis and aligning them with the wave vectors designated by α and β. It is obvious that one is proportional to the vertical vorticity, $\tilde{\eta}$, and the other is proportional to $\tilde{v}_y$ from (A.8):

$$\tilde{\eta} = i(\beta\tilde{u} - \alpha\tilde{w}), \quad (A.13)$$

$$\tilde{v}_y = -i(\alpha\tilde{u} + \beta\tilde{w}). \quad (A.14)$$

Applying this transformation to the equations, we obtain:

$$[\frac{\partial}{\partial t} + i(\alpha U + \beta W) - \frac{1}{Re}(\frac{\partial^2}{\partial y^2} - k^2)]\tilde{\eta} = i(\alpha W' - \beta U')\tilde{v}, \tag{A.15}$$

which is the Squire equation.

The original velocity components can be obtained from $\tilde{\eta}$ and $\tilde{v}_y$ as follows:

$$\tilde{u} = \frac{i}{k^2}(\alpha\tilde{v}' - \beta\tilde{\eta}), \tag{A.16}$$

$$\tilde{w} = \frac{i}{k^2}(\alpha\tilde{\eta} + \beta\tilde{v}'). \tag{A.17}$$

A.2 Falkner-Skan-Cooke transformation

J. C. Cooke [4] extended the Falkner-Skan transformation to flows over an infinite yawed wedge. The coordinate system is defined as follows: ξ-direction is parallel to the wedge and normal to the leading edge; ζ-direction is also parallel to the wedge surface and tangent to the leading edge. The flow over the wedge is divided into two components, U_c in the ξ-direction and W_c in the ζ-direction. U_c can be examined in the same manner as the normal Falkner-Skan transformation, where the velocity of the inviscid flow outside the boundary layer is given by;

$$U_i = U_{c0}(\xi)^m. \tag{A.18}$$

Since there is no pressure gradient in the ζ-direction;

$$W_i = W_{c0}, \tag{A.19}$$

where U_i, W_i, and the local sweep angle between the direction of the inviscid flow and the chord direction, ψ, satisfies the following equation:

$$\frac{W_i}{U_i} = \tan\psi. \tag{A.20}$$

Note that if $W_{c0} = 0$, this reduces to the two-dimensional case.

We define the variable as follows:

$$\eta = [\frac{(m+1)U_i}{2\nu\xi}]^{1/2} y, \tag{A.21}$$

$$U_c(\eta) = U_i f'(\eta), \tag{A.22}$$

$$W_c(\eta) = W_i g(\eta). \tag{A.23}$$

Using these variables and dropping the quadratic terms, the boundary-layer equations reduce to the following differential equations. g drops out of the equation for the flow in the ξ-direction, and the first equation becomes the familiar equation for the Falkner-Skan transformation, while the second equation is dependent on both f and g:

$$f''' + ff'' + H(1 - f'^2) = 0, \tag{A.24}$$

$$g'' + fg' = 0, \tag{A.25}$$

$$H = \frac{2m}{m+1}, \tag{A.26}$$

where H is the Hartree parameter, or $1/\pi$ of the wedge angle. The boundary conditions are:

$$f = f' = g = 0 \text{ when } \eta = 0, \tag{A.27}$$

$$f' \to 1, g \to 1 \text{ as } \eta \to \infty. \tag{A.28}$$

These equations were solved using Newton-Raphson method with 200 points in the y-direction.

We can use f' and g to construct the streamwise and crossflow velocity components. The mean flow profile $U(y)$ and $W(y)$ is given by;

$$U(\eta) = f'(\eta)\cos^2\psi + g(\eta)\sin^2\psi, \tag{A.29}$$

$$W(\eta) = [-f'(\eta) + g(\eta)]\cos\psi\sin\psi. \tag{A.30}$$

It is obvious that $W(\eta)$ have the same shape regardless of ψ, with maximum crossflow velocity at $\psi = 45^o$. However, $U(\eta)$ has a different shape depending upon ψ. For $\psi = 0^o$, $u(\eta) = f'(\eta)$; for $\psi = 90^o$, $u(\eta) = g(\eta)$.

The results were non-dimensionalized using δ^* calculated from $U(\eta)$ for use in numerical calculation.

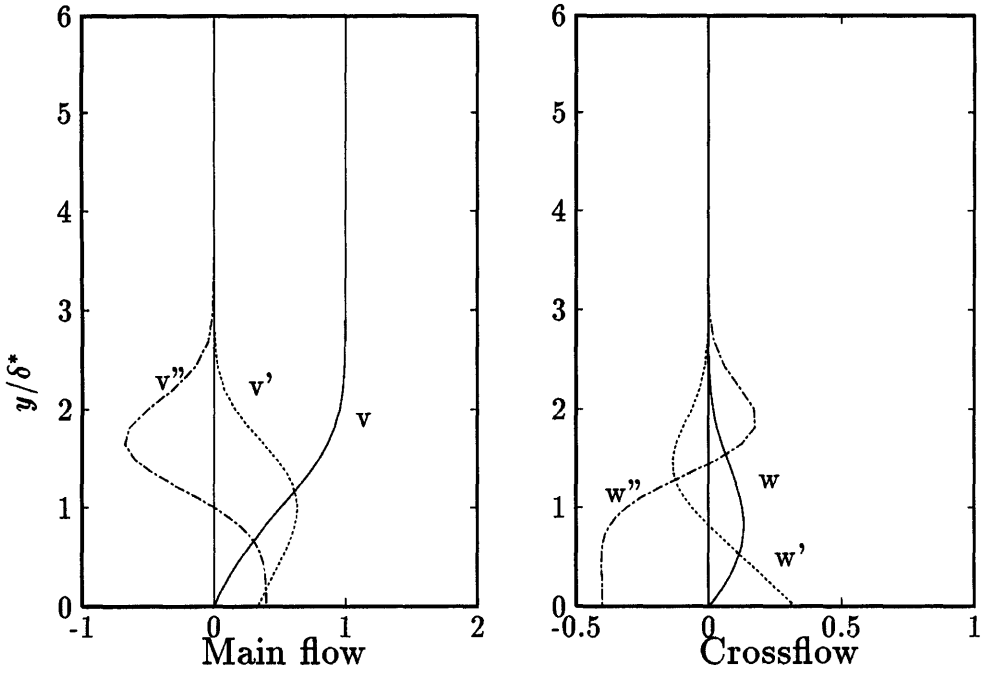

Figure A-1: Mean flow profile generated by Falkner-Skan-Cooke transform. $\psi = 45^0, H = -0.1988$

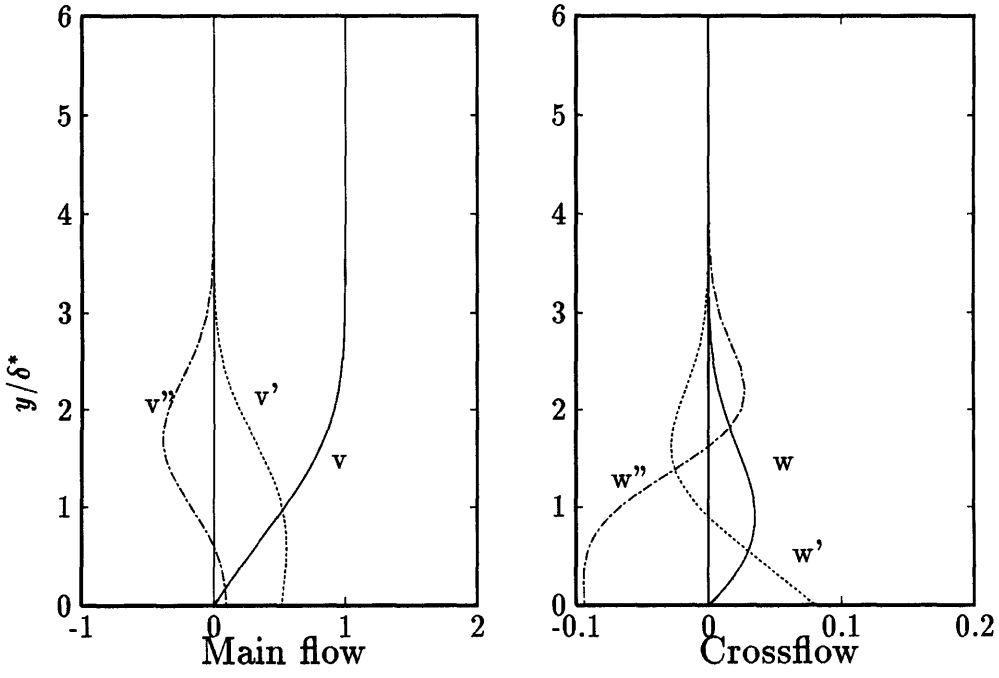

Figure A-2: Mean flow profile generated by Falkner-Skan-Cooke transform. $\psi = 45^0, H = -0.1$

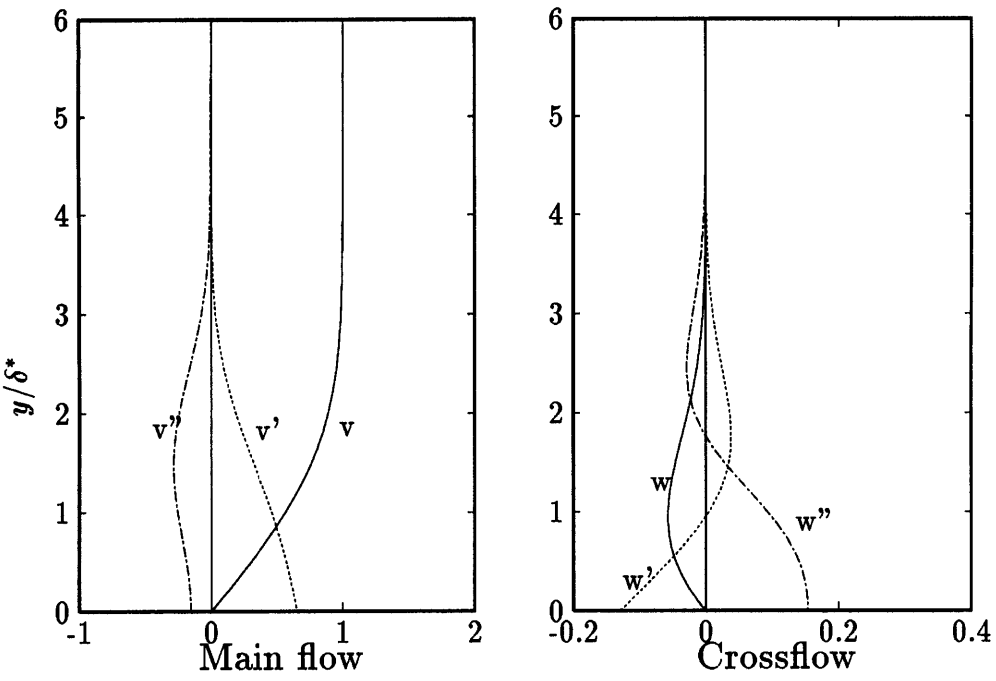

Figure A-3: Mean flow profile generated by Falkner-Skan-Cooke transform. $\psi = 45^0, H = 0.3$

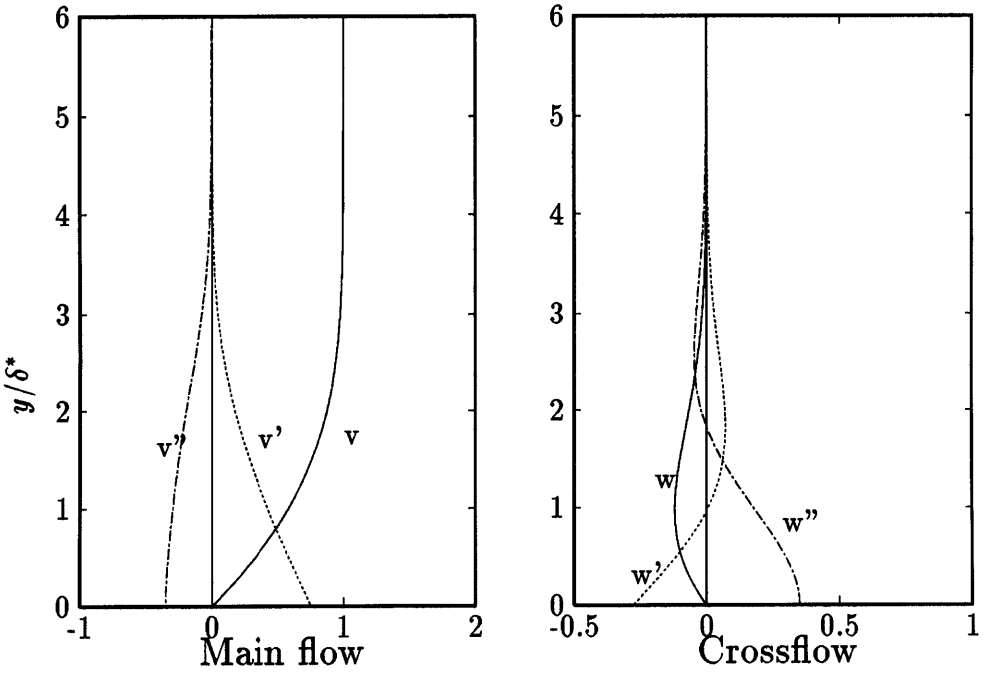

Figure A-4: Mean flow profile generated by Falkner-Skan-Cooke transform. $\psi = 45^0, H = 1.0$

Appendix B

Program Listings

The program listed is for calculating the evolution of a localized disturbance in three-dimensional boundary layer, showing all necessary steps for the computation. The program for examining individual Fourier modes was not given as it is very similar. The subroutine given is common to all the programs, and is used for reading in the boundary layer data and calculating the value at each Chebyshev collocation point.

```
      program localized_disturbance
c
c
c -- This program calculate the evolution of a localized
c -- disturbance.  The Fourier modes are integrated independently.
c -- The Orr-Sommerfeld and the Squire equations are integrated
c -- using LU method. The velocity and vorticity functions are
c -- decomposed using Chebyshev polynomials.
c -- The initial condition is two pairs of counter rotating
c -- vortices, but this can be modified very easily.
c
c -- Original program by Prof. K.S. Breuer, modified for viscosity,
c -- three-dimensional boundary layers, and Chebyshev approximation.
c
      implicit none

      integer nyd
      real  el, el1, el2, el3, pi, re
      parameter (nyd=64, pi=3.1415926535, re=950.0)
      parameter (el1=5.0, el2= 1.2, el3=6.0)

      real*8  yy(0:nyd), bl0(0:nyd), bl1(0:nyd), bl2(0:nyd)
      real*8  cf0(0:nyd), cf1(0:nyd), cf2(0:nyd), ymax
      real  u(0:nyd), up(0:nyd), upp(0:nyd)
      real  tt(0:nyd, 0:nyd, 0:4), r(0:nyd), s(0:nyd)
      real  q(0:nyd,0:nyd), d(0:nyd,0:nyd), dd(0:nyd, 0:nyd)
      integer indx1(0:nyd), indx2(0:nyd), indx3(0:nyd)
      complex*8 pc(0:nyd,0:nyd), qc(0:nyd,0:nyd), rc(0:nyd,0:nyd)
      complex*8 sc(0:nyd,0:nyd), basc(0:nyd,0:nyd)
      complex*8 vorp(0:nyd), vnp(0:nyd), vp(0:nyd)
      complex*8 vn(0:nyd), vor(0:nyd), ci, dummy
      real alpha_min, beta_min, alpha, beta, ak
      real elx, elz, a1, b1, dy, d2, d4, y, y2
      real dt, t, tmax, tstart, fac, step
      integer   i, j, k, ia, ib, id, iy, ny, na, nb, inread
      real      fpread
      character*8 filein, fileout
      logical restart, iver
      ci = cmplx(0.0, 1.0)
c
c
c --
      if (iver('Start from T=0 ? '))then
         restart = .false.
 5       ny = inread('Points in y direction [max 64]')
```

```
         if (ny .gt. nyd) goto 5
         el = 1.0
c         el = fpread('Mapping factor 1')
         ymax = dble(el)
         call setup(ny, yy, bl0, bl1, bl2, cf0, cf1, cf2, ymax)
         na = 32
c 15      na=inread('Number of alpha to calculate [max 64]')
c         if (na .gt. 64) goto 15
         elx = 200.0
c         elx=fpread('Box length ')
         alpha_min=2.*pi/elx
         nb = 16
c 25      nb=inread('Number of beta to calculate  [max 64]')
c         if (nb .gt. 64) goto 25
         elz = 50.0
c         elz=fpread('Box width  ')

         beta_min=2.*pi/elz
         tstart = 0.0
      else
         restart=.true.
         call stread('Name of restart file ',filein)
         open(unit=2, file=filein, status='old', form='unformatted')
         read(2) na, nb, elx, elz
         read(2) dt, tstart, ny, el
         ymax = dble(el)
         call setup(ny, yy, bl0, bl1, bl2, cf0, cf1, cf2, ymax)
         write(6,*)'Starting time ',tstart
         write(6,*)
         call prtint('# of Alpha    ',na)
         call prtint('# of Beta     ',nb)
         write(6,*)'Box length    ',elx
         write(6,*)'Box width     ',elz
         alpha_min=2.*pi/elx
         beta_min=2.*pi/elz
      endif
c
c
      dt=fpread('Time step   ')
      tmax=fpread('Max time to integrate to ')
      write(6,*)
      write(6,*)'Alpha min ',alpha_min
      write(6,*)'      max ',na*alpha_min
      write(6,*)'Beta  min ',beta_min
      write(6,*)'      max ',nb*beta_min
```

```
c
 35   call stread('Name of output file ',fileout)
      if (fileout .eq. filein) goto 35
c
      open(unit=1,file=fileout,status='unknown',form='formatted')
      rewind(1)
      write(1,*) na, nb, ny, el
      write(1,*) dt, tmax, elx, elz
      write(6,*)
      write(6,*)na, nb, alpha_min, beta_min, dt, tmax, ny
c
c -- Set up Chebyshev polynomials matrix T and its derivatives
c
      do k = 0, ny
         do j = 0, ny
            tt(j,k,0) = cos(j*k*pi/ny)
         enddo
      enddo
c
      do id = 1,4
         do j = 0, ny
            tt(j,0,id) = 0.0
            tt(j,1,id) = tt(j,0,id-1)
            tt(j,2,id) = 4. * tt(j,1,id-1)
            do k = 3, ny
               tt(j,k,id) = 2.*k*tt(j,k-1,id-1) + k*tt(j,k-2,id)/(k-2)
            enddo
         enddo
      enddo
c
c -- Set up the base matrix for decomposition to coefficients
c
      do k=0,ny
         do j = 0,ny
            basc(j,k) = cmplx(tt(j,k,0), 0.0)
         enddo
      enddo
      call c_ludcmp(basc, ny+1, nyd+1, indx3, dummy)
c
c -- Loop through the wave numbers...Main part
c
      do ia=1,na
         alpha=alpha_min*ia
         do ib=1,nb*2
            beta=beta_min*(ib-nb)
```

```
            ak = sqrt(alpha**2 + beta**2)
            write(6,200) ia, ib, alpha, beta, ak
c
c -- Set the velocity profiles -- up is set up differently
c
            do j = 0, ny
               u(j) = alpha*sngl(bl0(j))+beta*sngl(cf0(j))
               up(j) = beta*sngl(bl1(j))-alpha*sngl(cf1(j))
               upp(j) = alpha*sngl(bl2(j))+beta*sngl(cf2(j))
            enddo
c
c -- First get the initial velocity.
c
            if (restart) then
               do i = 0,ny
                  read(2,*) fac, vn(i)
                  read(2,*) vp(i), vor(i)
               enddo
            else
c
c -- Generate initial velocity using two pairs of
c -- counter-rotating vortices.  This portion can easily be
c -- replaced with any initial condition.
c
               a1 = alpha*el1
               b1 = beta*el3
               fac = -a1*b1*exp((-a1**2 - b1**2)/4.0)
               do j = 0,ny-1
                  y = sngl(yy(j))/el2
                  y2 = y*y
                  if (y2 .lt. 50.0) then
                     vn(j) = fac * ci * b1 * exp(-y2) * y**3
                     vor(j) = -fac*ci*a1 * exp(-y2) * y2*(3.0-2.0*y2)
                  else
                     vn(j) = cmplx(0.0, 0.0)
                     vor(j) = cmplx(0.0, 0.0)
                  endif
               enddo
               vn(ny) = cmplx(0.0,0.0)
               vor(ny)= cmplx(0.0,0.0)
               call c_lubksb(basc, ny+1, nyd+1, indx3, vn)
               call c_lubksb(basc, ny+1, nyd+1, indx3, vor)
            endif
c
c -- Assemble the solver matrix
```

```
c
            do k = 0, ny
               do j = 1, ny-1
                  fac = (cos(j*pi/ny)+1)/2
                  d2 = 4*fac**3 * (fac*tt(j,k,2) + tt(j,k,1)) /el/el
                  d(j,k) = d2 - ak**2 * tt(j,k,0)
                  d4 = (16*fac**5) * (((fac*tt(j,k,4)+6*tt(j,k,3))*
     &                 fac+9*tt(j,k,2))*fac+3*tt(j,k,1)) / el**4
                  dd(j,k) = d4 - 2 * ak**2 * d2 + ak**4 * tt(j,k,0)
               enddo
            enddo
            do j = 1,ny-1
               r(j) = dt*u(j)/2.0
               s(j) = dt*upp(j)/2.0
            enddo
            do k = 0, ny
               do j=1, ny-1
                  q(j,k) = r(j)*d(j,k) - s(j)*tt(j,k,0)
               enddo
            enddo
c
c -- Viscosity factor. For inviscid case, set this to 0
c            fac = 0.0
            fac = dt / re / 2.0
c
c -- Assemble the left hand and right hand sides for vn (velocity)
c
            do k = 0, ny
               do j = 1, ny-1
                  pc(j,k) = cmplx(d(j,k) - fac*dd(j,k), q(j,k))
                  qc(j,k) = cmplx(d(j,k) + fac*dd(j,k), -q(j,k))
               enddo
c
c -- Boundary conditions v = v' = 0 at y = 0, and y = infinity
c
               pc(0,k) = cmplx(tt(0,k,0), 0.0)
               pc(1,k) = cmplx(tt(0,k,1), 0.0)
               pc(ny-1,k) = cmplx(tt(ny,k,0), 0.0)
               pc(ny,k) = cmplx(tt(ny,k,1), 0.0)
               qc(0,k) = cmplx(0.0, 0.0)
               qc(1,k) = cmplx(0.0, 0.0)
               qc(ny-1,k) = cmplx(0.0, 0.0)
               qc(ny,k) = cmplx(0.0, 0.0)
            enddo
c
```

```
c -- Assemble the matrices for solving vor (vorticity)
c
            do k = 0,ny
               do j = 1,ny-1
                  rc(j,k)=cmplx(tt(j,k,0)-fac*d(j,k),r(j)*tt(j,k,0))
                  sc(j,k)=cmplx(tt(j,k,0)+fac*d(j,k),-r(j)*tt(j,k,0))
               enddo
            enddo
c
c -- Boundary conditions vor = 0 at y = 0 and y = infinity
c
            do k = 0,ny
               rc(0,k) = cmplx(tt(0,k,0), 0.0)
               rc(ny,k) = cmplx(tt(ny,k,0), 0.0)
               sc(0,k) = cmplx(0.0, 0.0)
               sc(ny,k) = cmplx(0.0, 0.0)
            enddo
c
c -- Iterate in time.
c
            t = tstart
c
c -- The initial LU decomposition for the O-S and Squire
c -- equations matrices
c
            call c_ludcmp(pc, ny+1, nyd+1, indx1, dummy)
            call c_ludcmp(rc, ny+1, nyd+1, indx2, dummy)
            do while(t .lt. tmax)
               t = t + dt
c
c -- Calculate coefficients vnp (velocity) with LUD matrix pc
c
               do j = 0, ny
                  vnp(j) = cmplx(0.0,0.0)
                  do k = 0, ny
                     vnp(j) = vnp(j) + qc(j,k) * vn(k)
                  enddo
               enddo
c
c -- LU back substitution of the O-S equation
c
               call c_lubksb(pc, ny+1, nyd+1, indx1, vnp)
c
c -- Calculate coefficients vorp (vorticity) with LUD matrix rc
c
```

```
               do j = 0,ny
                  vorp(j) = cmplx(0.0,0.0)
                  do k = 0,ny
                     vorp(j) = vorp(j) + sc(j,k) * vor(k) +
     &                    ci*dt*up(j)/2 * tt(j,k,0) * (vn(k)+vnp(k))
                  enddo
               enddo
c
c -- LU back substitution of the Squire equation
c
               call c_lubksb(rc, ny+1, nyd+1, indx2, vorp)
c
c -- Put in the new values
c
               do j = 0,ny
                  vn(j)=vnp(j)
                  vor(j)=vorp(j)
               enddo
            enddo
c
c -- end of time iteration
c
c -- Calculate the actual derivative of velocity v'
c
            do j = 0,ny
               fac = -2.0*((cos(j*pi/ny)+1.0)/2.0)**2/el
               vp(j) = 0.0
               do k = 0,ny
                  vp(j) = vp(j) + vn(k)*fac*tt(j,k,1)
               enddo
            enddo
            call c_lubksb(basc, ny+1, nyd+1, indx3, vp)
c
c -- Write array to disk
c
            do j = 0,ny
               write(1,*) j, vn(j)
               write(1,*) vp(j), vor(j)
            enddo
         enddo
      enddo
      close(1)
      close(2)

 200  format('IA: ',i3,' IB: ',i3,' Alpha: ',f6.2,
```

```
     &      ' Beta: ',f6.2,' K: ',f6.2)
c
       end
```

```
      subroutine setup(n, ynew, bl0, bl1, bl2, cf0,cf1,cf2,ybl)
c
c -- This subroutine read in the mean streamwise and crossflow
c -- velocity profile and give them back at Chebyshev collocation
c -- points.
c
      double precision pi
      integer nyd, nmax
      parameter (nyd = 128,nmax=200,pi=3.141592653589793d0)

      real*8  ynew(0:nyd), bl0(0:nyd), bl1(0:nyd), bl2(0:nyd)
      real*8  cf0(0:nyd), cf1(0:nyd), cf2(0:nyd), ybl
      real*8  qb(0:nmax), qc(0:nmax), qd(0:nmax)
      real*8  qe(0:nmax), qf(0:nmax)
      real*8  temp1(0:nmax), temp2(0:nmax), temp3(0:nmax)
      real*8  y(0:nmax), yy, bmin, bmax, umax, ymax
      real*8  sxi, phi, el
      real*8  d_quintint
      integer i, k, j, n, ny
      character filein*20
c
      if (n .gt. nyd) then
         write(*,*) 'nyd too small in setup subroutine'
         stop
      endif
      el = ybl
c -- read in the Blasius profile
      open(unit=2, file='Info', status='old', form='formatted')
      read(2,*)
      read(2,*) filein
      close(2)
c
c      write(6,*) filein
      open(unit=1,file=filein,status='old',form='formatted')
      read(1,*) ny
c      write(6,*) 'number of points ',ny
      do i = 0, ny
         read(1,*) y(i), temp1(i), temp2(i), temp3(i)
      enddo
c
c -- Normalize the profile
      umax = 0.0d0
      ymax = 0.0d0
      do k = 0, ny
         umax = max(umax, temp1(k))
```

```
         ymax = max(ymax, y(k))
      enddo
c
c -- Fit a quintic spline to the velocity profile
      call d_quinat(ny+1, y, temp1, qb, qc, qd, qe, qf)
c -- Interpolate to Chebyshev points
      do k = 0, n-1
         sxi = dcos(k*pi/n)
         yy = min(ymax, el * (1 - sxi) / (1 + sxi))
         bl0(k) = d_quintint(yy, ny+1, y, temp1,
     $        qb, qc, qd, qe, qf)/umax
         ynew(k) = min(k*1.0d5, el * (1 - sxi) / (1 + sxi))
      enddo
      bl0(n) = d_quintint(ymax, ny+1, y, temp1,
     $     qb, qc, qd, qe, qf)/umax
      ynew(n) = n*1.0e5
c
c -- First derivative
      call d_quinat(ny+1, y, temp2, qb, qc, qd, qe, qf)
      do k = 0, n-1
         sxi = dcos(k*pi/n)
         yy = min(ymax, el * (1 - sxi) / (1 + sxi))
         bl1(k) = d_quintint(yy, ny+1, y, temp2,
     $        qb, qc, qd, qe, qf)/umax
      enddo
      bl1(n) = d_quintint(ymax, ny+1, y, temp2,
     $     qb, qc, qd, qe, qf)/umax
c
c -- Second derivative
      call d_quinat(ny+1, y, temp3, qb, qc, qd, qe, qf)
      do k = 0, n-1
         sxi = dcos(k*pi/n)
         yy = min(ymax, el * (1 - sxi) / (1 + sxi))
         bl2(k) = d_quintint(yy, ny+1, y, temp3,
     $        qb, qc, qd, qe, qf)/umax
      enddo
      bl2(n) = d_quintint(ymax, ny+1, y, temp3,
     $     qb, qc, qd, qe, qf)/umax
c
c -- read in the crossflow profile
      read(1,*)
      do i=0,ny
         read(1,*) y(i), temp1(i), temp2(i), temp3(i)
      enddo
      close(1)
```

```
c -- Fit a quintic spline to the velocity profile
      call d_quinat(ny+1, y, temp1, qb, qc, qd, qe, qf)
      do k = 0, n-1
         sxi = dcos(k*pi/n)
         yy = min(ymax, el * (1 - sxi) / (1 + sxi))
         cf0(k) = d_quintint(yy, ny+1, y, temp1,
     $        qb, qc, qd, qe, qf)/umax
      enddo
      cf0(n) = d_quintint(ymax, ny+1, y, temp1,
     $     qb, qc, qd, qe, qf)/umax

c -- First derivative
      call d_quinat(ny+1, y, temp2, qb, qc, qd, qe, qf)
      do k = 0, n-1
         sxi = dcos(k*pi/n)
         yy = min(ymax, el * (1 - sxi) / (1 + sxi))
         cf1(k) = d_quintint(yy, ny+1, y, temp2,
     $        qb, qc, qd, qe, qf)/umax
      enddo
      cf1(n) = d_quintint(ymax, ny+1, y, temp2,
     $     qb, qc, qd, qe, qf)/umax

c -- Second derivative
      call d_quinat(ny+1, y, temp3, qb, qc, qd, qe, qf)
      do k = 0, n-1
         sxi = dcos(k*pi/n)
         yy = min(ymax, el * (1 - sxi) / (1 + sxi))
         cf2(k) = d_quintint(yy, ny+1, y, temp3,
     $        qb, qc, qd, qe, qf)/umax
      enddo
      cf2(n) = d_quintint(ymax, ny+1, y, temp3,
     $     qb, qc, qd, qe, qf)/umax
c
      return
c
      end
```

Bibliography

[1] Kenneth S. Breuer and Richard M. Everson. On the errors incurred calculating derivatives using chebyshev polynomials. *J. of Computational Physics*, 99(1), 1992.

[2] Kenneth S. Breuer and Joseph H. Haritonidis. The evolution of a localized disturbance in a laminar boundary layer. Part 1. Weak disturbances. *J. of Fluid Mech.*, 220, 1990.

[3] Kathryn M. Butler and Brian F. Farrell. Three-dimensional optimal perturbations in viscous shear flow. *Phys. Fluids*, 4(8), 1992.

[4] J. C. Cooke. The boundary layer of a class of infinite yawed cylinders. *Proceedings of Cambridge Phil. Soc. Vol. 46*, 1950.

[5] A. D. D. Craik. Nonlinear resonant instability in boundary layers. *J. of Fluid Mech.*, 50, 1971.

[6] W. E. Gray. The effect of wing sweep on laminar flow. *RAE TM Aero*, 255, 1952.

[7] C. E. Grosch and H. Salwen. The continuous spectrum of the orr-sommerfeld equation. part 1. the spectrum and the eigenfunctions. *J. of Fluid Mech.*, 87, 1978.

[8] L. Håkan Gustavsson. Initial-value problems for boundary layer flows. *Phys. Fluids*, 22(9), 1979.

[9] L. Håkan Gustavsson. Energy growth of three-dimensional disturbances in plane Poiseuille flow. *J. of Fluid Mech.*, 224, 1991.

[10] Dan S. Henningson. An eigenfunction expansion of localized disturbances. *Advances in Turbulence*, 3, 1991.

[11] T. Herbert. Analysis of the subharmonic route to transition in boundary layers. AIAA Paper 84-0009, 1984.

[12] Lennart S. Hultgren and L. Håkan Gustavsson. Algebraic growth of disturbances in a laminar boundary layer. *Phys. Fluids*, 24(6), 1980.

[13] P. S. Klebanoff, K. D. Tidstrom, and L.M. Sargent. The three-dimensional nature of boundary layer instability. *J. of Fluid Mech.*, 12, 1962.

[14] M. T. Landahl. Wave breakdown and turbulence. *SIAM J. of Appl. Maths*, 28, 1975.

[15] Leslie M. Mack. Boundary layer linear stability theory. *Special Course on Stability and Transition of Laminar Flow, AGARD Report*, 709, 1984.

[16] Peter L. O'Sullivan and Kenneth S. Breuer. Transient Growth of Non-Axisymmetric Disturbances in Laminar Pipe Flow. FDRL TR 93-1, Massachusetts Institute of Technology, February 1993.

[17] William H. Press, Brian P. Flannery, Saul A. Teukolsky, and William T. Vetterling. *Numerical Recipes, The Art of Scientific Computing [FORTRAN version].* Cambridge University Press, 1989.

[18] Helen L. Reed and William S. Saric. Stability fo three-dimensional boundary layers. *Ann. Rev. Fluid Mech.*, 21, 1989.

[19] L. Rosenhead. *Laminar Boundary Layers.* Oxford University Press, 1963.

[20] J. M. Russell and M. T. Landahl. The evolution of a flat eddy near a wall in an inviscid shear flow. *Phys. Fluids*, 27, 1984.